Article

Nonlinear Soil–Pile–Structure Interaction Behaviour of Marine Jetty Structures

Marios Koronides [1], Constantine Michailides [2,*] and Toula Onoufriou [1]

1   Department of Civil Engineering and Geomatics, Cyprus University of Technology, 3036 Limassol, Cyprus; marios.koronides@cut.ac.cy (M.K.); t.onoufriou@cut.ac.cy (T.O.)
2   Department of Civil Engineering, International Hellenic University, 621 24 Serres, Greece
*   Correspondence: cmichailides@ihu.gr

Abstract: Nonlinear soil–pile–structure interaction (SPSI) phenomena are known to play a vital role in the response of bottom-fixed marine structures. For such structures, these phenomena are commonly considered by the imposition of p-y, τ-z, and q-z springs, representing the lateral and axial shaft and axial base soil resistances, respectively. The importance of each resistance mechanism depends on the type of foundation system, with only very limited studies investigating their roles in the response of piled marine structures, such as jetties. Within this context, this study presents numerical three-dimensional pushover analysis results for two marine jetties, a smaller model with four piles and a larger model supported by twenty-four piles. SPSI effects are considered through p-y, τ-z, and q-z springs, the behaviours of which are determined by following commonly employed procedures. The structures' responses are investigated under the influence of various assumptions regarding the behaviours of springs, as well as steel plasticity. The current investigation underscores the substantial influence of the axial soil–pile interaction on the response of the jetty, particularly in terms of its failure mode. Moreover, it demonstrates the importance of incorporating p-y springs, even though the choice between their linear or nonlinear constitutive behaviour is found to be less critical. Finally, the study concludes that the behaviours of the springs significantly affect the system's ductility and the degree of steel yielding in the piles, while also highlighting the unconservative influence of neglecting SPSI phenomena.

Keywords: marine structures; marine jetties; soil–pile–structure interaction; finite element analysis; pushover simulations; τ-z, q-z, and p-y springs; axial soil–pile interaction; steel plasticity; ductility

1. Introduction

Bottom-fixed marine structures are usually founded on piles driven deep below the seabed. The response of the structures can be highly nonlinear due to structural nonlinearity, soil nonlinearity, and geometric nonlinearity. With respect to foundation design, soil is commonly assumed to be rigid [1,2], i.e., fixed conditions at the seabed level, or foundation compliance is accounted through linear elastic springs [3–5]. However, as it is well known, soil behaves nonlinearly even at small strains under either static or cyclic loading [6–9], affecting the response of the structure. The interaction between the structural response and piled foundations is commonly referred to as soil–pile–structure interaction (SPSI). SPSI effects can reduce the base shear and ultimate strength, and increase the structural displacements in comparison with the ones that would have occurred when foundation is assumed rigid [3,10]. When displacements become large, P-Δ phenomena can render SPSI effects detrimental, making their neglect unconservative [11,12]. Therefore, it comes to no surprise that, despite the fact that Eurocode 8 [13] does not give specific guidelines towards the consideration of soil–structure–interaction phenomena, it requires their consideration in structures that are prone to P-Δ effects.

Nonlinear SPSI effects can be considered through numerical analyses by placing distributed nonlinear springs along the embedded piles or by explicitly modelling soil

with finite elements. The latter approach can be more rigorous when it employs advance soil constitutive modes that account for soil nonlinearity from small to large strains [8,14] and interface elements at pile–soil interfaces to enable gap formation and sliding [15,16]. However, due to its complexity, this approach is less frequently used in marine structure studies compared to the simpler and more effective use of nonlinear springs. The approach using springs is commonly referred to as Winkler idealization. It can involve springs acting in all three directions, representing soil reactions (known as subgrade) due to piles' lateral and axial deformation modes. There are three types of springs that can be used in numerical models. p-y springs aim to represent the soil subgrade reaction, p, due to lateral pile displacement, y. Axial springs, τ-z and q-z, express the shaft, τ, and base, q, resistances of soil due to the pile's vertical displacement, z.

The p-y springs have been extensively employed in monopile foundations [4,5,17] and can be defined using various formulations that exist in the literature [18–23]. More recently, more advanced p-y springs have been developed to account for gapping effects likely to occur in cohesive materials [24–27]. Other studies propose p-y springs that consider soil stiffness degradation as strains increase, particularly at small strain levels [28,29]. Axial springs have found wide applicability in designing jacket foundations [3,10,30–33], where the axial behaviour of the soil–pile interaction is of primary importance. As mentioned by Wen [34], axial subgrade reactions are instrumental in capturing the progressive failure mechanism and in estimating various aspects such as a pile's axial capacity, as well as the distribution of load and settlement along the pile's length. The same study summarizes existing formulations, with the one proposed by Randolph and Worth [35] being the most widely used.

The impact of soil compliance nonlinearity on marine structures is well established from very small strains [4,17], i.e., a linear response, to large strains [36,37]. By comparing existing subgrade reaction p-y models to represent the linear behaviour of soil, Prendergast and Gavin [17] and Damgaard et al. [4] have shown a sensitivity of the natural period of an offshore monopile to the adopted model. As mentioned by Abhinav and Saha [3], when linear springs are used to represent soil resistance in larger strain problems, the capacity of elastoplastic marine structures can be significantly overestimated. Zeng at al. [36] further investigated the impact of constitutive behaviour of p-y springs on offshore monopiles, concluding a need to consider the p component resulting from pile–soil friction during lateral loading. In fact, they observed that when this component is neglected, the magnitude and the position of the bending moment acting on monopiles might not be predicted accurately. Similarly, Chigullapally et al. [37] have shown that the location of the maximum bending moment acting on a bridge pier can shift upwards when increasing the ultimate p stress of shallow layers. The same study showed also the significant impact of the compliance and nonlinearity of the surface soft clay layer on the overall system's lateral response. The observations made by the latter authors align with those made by Asgarian and Lesani [38], who emphasized the highly nonlinear behaviour of the shallow soil layers and its impact on the overall static response of a jacket foundation.

Additionally, the impact of soil nonlinearity on offshore wind turbines when soil strains are within the small stain range and far from yielding has been found to be significant under circumstances. Hanssen [29] have shown that for small strain problems, p-y springs that account for soil stiffness variations at small strains are more suitable than the more commonly used springs (e.g., API [39]) that neglect this variation. The same author also showed that for larger strain problems, the former springs do not provide a significant benefit when used for shallow soil layers due to large strains, while a small benefit might be present when used for deeper soil layers. More recently, Zhu [28] compared results from analyses that use either API's p-y springs or more sophisticated springs that account for soil stiffness degradation at small strains. The outcome of the study is that the utilization of API's springs might lead to an overestimation of soil resistance at small displacements and underestimation at large.

The nonlinear behaviour and ultimate capacity of marine structures, including offshore bottom-fixed platforms and jacket structures, is commonly evaluated by the means of pushover analyses [3,10,15,33,38]. The use of these analyses, which can be either static or dynamic, is suggested by the widely adopted API [39] and DNV [40] guidelines. The pushover approach is used to verify that the capacity of SPSI systems exceeds the ultimate design loads (e.g., wave, current, wind, or earthquake loads), ensuring their safety. It has also found applicability in identifying the critical structural members and failure modes of marine structures. Abhinav and Saha [3] have shown that in marine structures, neglecting SPSI effects can obscure failure modes, as failure can be associated with soil failure rather than structural yielding. Yee et al. [41] employed pushover analyses to ensure the sustainability of existing structures in response to aging effects, which, as shown by Wen et al. [31], can have a positive impact on the shaft capacity of piles. Additionally, results from pushover analyses were exploited by Rahnami et al. [42] for determining p-y springs.

The above discussion demonstrates the significant impact of SPSI and soil nonlinearity on the response and capacity of marine structures. However, relevant experimental and numerical studies on bottom-fixed marine jetties and platforms are scarce. Especially, there are limited, if any, studies that investigate the role of each resistance mechanism, shaft, base, and lateral, on the responses of such structures [43]. Such structures usually serve the energy sector, such as oil and gas companies, rendering them critical infrastructure for the operational stability of their respective countries. Due to confidentiality concerns, oil and gas companies often do not share data, contributing to the scarcity of relevant studies, particularly those validated based on real data.

Within this context, this study presents three-dimensional (3D) parametric static pushover analyses of a marine jetty with varied assumptions regarding τ-z, q-z, and p-y springs, as well as steel plasticity. The jetty is representative of an existing structure located in Vasiliko in Cyprus, while geological and geotechnical information is based on information provided by a relevant infrastructure owner with operations in the Vasiliko area in Cyprus. The examined jetty is founded on 24 open-ended inclined piles driven to a maximum depth of 26.35 m below the seabed. Prior to investigating this structure, a simpler marine structure with four inclined piles is also examined using the same foundation data. The aim of these analyses is to facilitate comprehension of resistance mechanisms, which is used to interpret the response of the more complex jetty.

The soil–pile interaction is considered through p-y springs placed along the two horizontal directions, as well as the vertical τ-z and q-z springs placed along the shaft and at the piles' base, respectively. Springs' force–displacement behaviour is prescribed based on API's [39] guidelines, except for p-y springs for stiff clay, for which the formulation proposed by Reese et al. [21] is followed. Aiming to investigate the importance of each nonlinear mechanism, all springs behave either linearly or nonlinearly, while p-y springs can even be neglected entirely. The present study highlights the significant role of the axial soil–pile interaction on the jetty response, emphasizing on its role on the failure mode. Concurrently, it indicates the necessity of incorporating p-y springs even though the choice of their constitutive behaviour is found less important. Finally, it is concluded that the choice of springs' behaviours influences the system's ductility and the extent of steel yielding in the piles.

2. Structural Characteristics

The examined structure is a bottom-fixed marine platform that is representative of a T-junction of a marine jetty, such as the one depicted in Figure 1, located in the Vasiliko area in Cyprus. The T-junction is assumed to connect along its short axis two transverse components (trestles) and one longitudinal component along its long axis (see Figure 1a, b). The transverse components host four berths, each capable of hosting a large vessel. The T-junction will also be utilized for loading and unloading operations. Given the structural role of the T-junction, combined with the operational activities, as well as wave and seismic

loading, it is expected that substantial lateral and vertical forces will be exerted on the SPSI system. These forces are anticipated to induce a highly nonlinear response in the system, which is investigated herein. The behaviour of such marine structures is of particular interest, given the fact that they can comprise significant elements of the country's, Cyprus in particular, energy infrastructure.


(a)
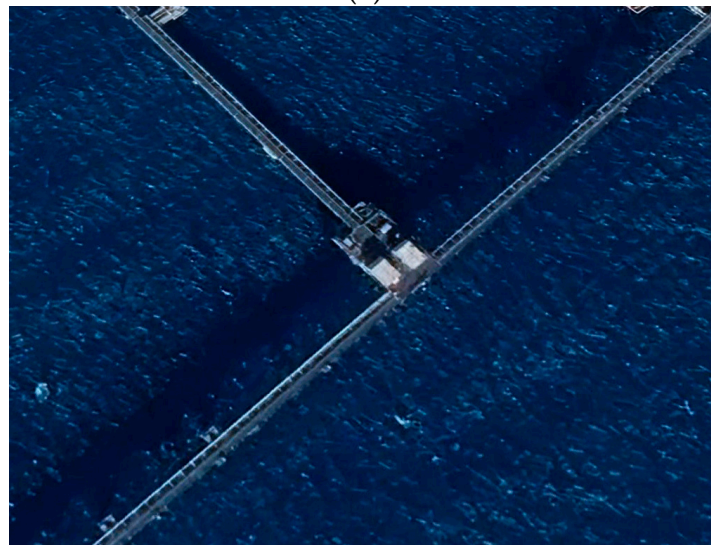
(b)

Figure 1. Reference marine structure located in the Vasiliko area in Cyprus. (**a**) Aerial view of the jetty, and (**b**) aerial view focusing on the T-junction.

The assumed platform consists of a 1.30 m thick C35/45 reinforced concrete deck with dimensions of 32 m × 20 m in plan and a piled foundation system comprising 24 inclined steel piles. Figure 2 illustrates the positions and inclination direction of the piles below the deck, with the inclination characterized by a rake of 1:3. The piles are assumed to have a hollow circular cross-sectional area with a diameter of 1067 mm and a thickness of 27 mm, complying with the requirements of class 3 cross-sectional areas. The steel material complies with the API L5 grade X65 and has yield (f_y) and ultimate (f_u) stresses of 450 MPa and 550 MPa, respectively.

Piles of three different lengths, 42.7 m, 45.4 m, and 54.3 m, were driven in the soil by the means of the impact method, with the pile ends reaching depths of 15.35 m, 17.85 m, and

26.35 m, respectively. As illustrated in Figure 2, the piles of shorter length were placed at the deck's edges, while the longest piles were placed near the centre of gravity of the deck.

The underside of the concrete deck lies on 7.5 m above the mean sea level. Below this elevation, the piles are connected to the concrete slab through a concrete plug, with the first 2.4 m of piles behaving as composite material. The composite parts of piles are expected to exhibit considerably higher stiffness than the remaining piles. Nonetheless, assumptions regarding their stiffness are necessary due to the absence of additional information.
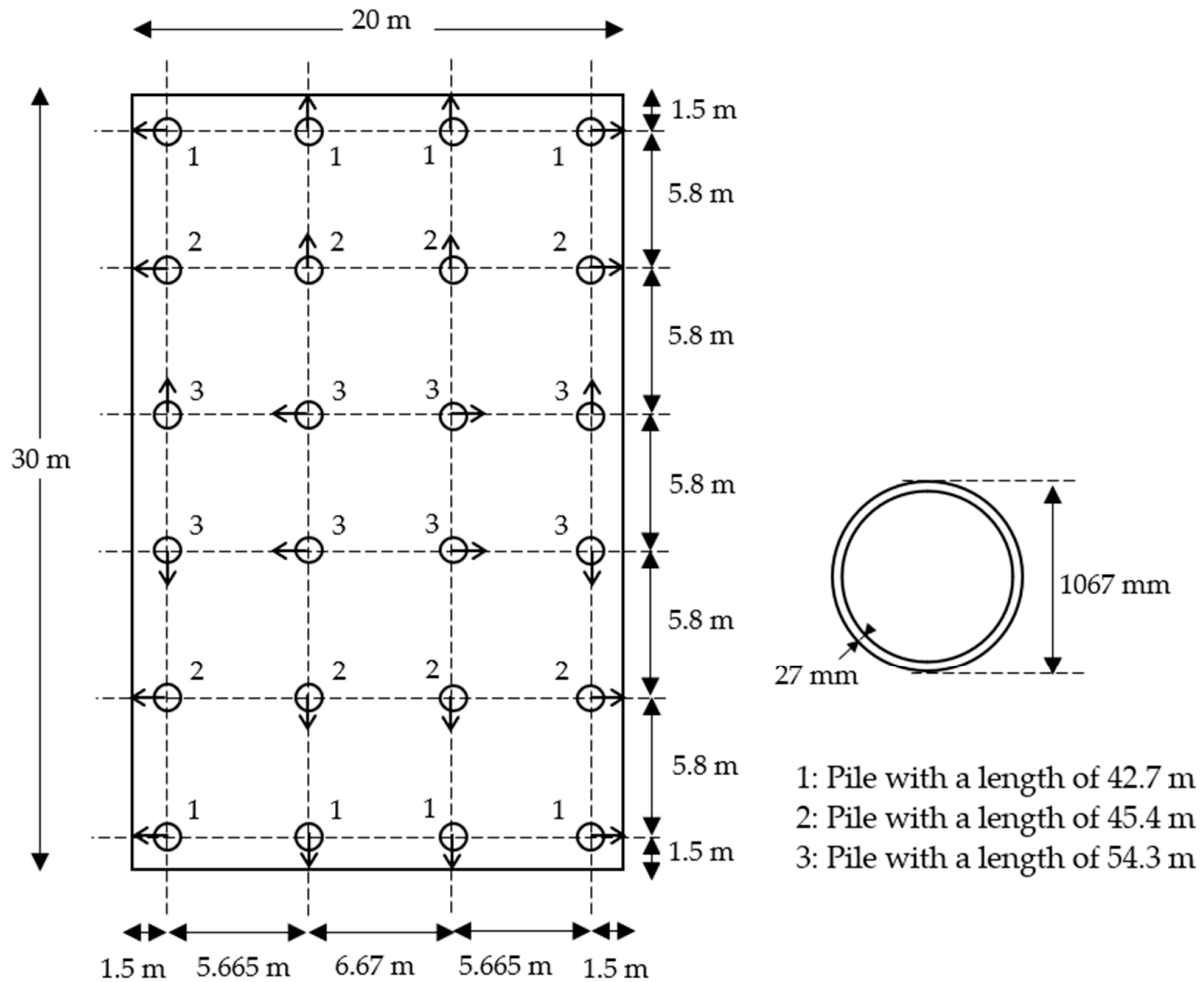
Figure 2. Underside view of the connections of the piles with the deck of the platform illustrating schematically the positions and the direction of inclination of the piles. The cross-sectional area and the length of the piles are also provided.

3. Site Conditions

The examined marine structure is assumed to be founded at the site of the reference jetty in Vasiliko area, which is a site hosting critical energy infrastructure for Cyprus. The structure is located at approximately 1.2 km far from the seashore, where the seabed lies 17.7 m below sea level. Geotechnical and geological information for the site were provided by VTTV, a marine energy infrastructure owner of a marine jetty in the Vasiliko area of Cyprus [44].

The geotechnical investigation campaign was carried out prior to the construction of the reference jetty. The investigation included borehole drilling, in situ SPT tests and various lab tests, such as particle size distribution, bulk and dry density tests, natural moisture, unconfined compressive strength tests, Atterberg limits and linear shrinkage tests. For all tests, the British Standards were followed [45,46]. Boring was conducted by the means of the rotary percussion drilling method with the aid of a jack-up platform. During

drilling, SPT tests were carried out, and samples were also retrieved through driving a split spoon barrel sampler. Undisturbed samples were taken from the identified rock formation using a sampler driven by static pressure of the drill rig or by blows of the SPT hammer.

The investigation revealed three types of soil: fine grained cohesionless sandy/silty/clay soil, coarse grained–gravelly soil, and Nicosia marl. The soil stratigraphy is provided in Figure 3. As the figure shows, fines encountered in the first 1.5 m are characterized as loose sand, which was found to be of very low stiffness, and therefore this layer is disregarded in the ensuing sections. The second and third layers are characterized as dense sand with gravels, while lab data indicated low plasticity, with a plasticity index (PI) ranging between 0 and 15%. SPT tests at this layer provided N-SPT values mostly larger than 60 per 30 cm of settlement at six offshore boreholes along the length of the jetty. Specifically, at a borehole below the T-junction, 30 cm of settlement was not reached after 100 blows, indicating that the gravelly sand layer is of very high stiffness.
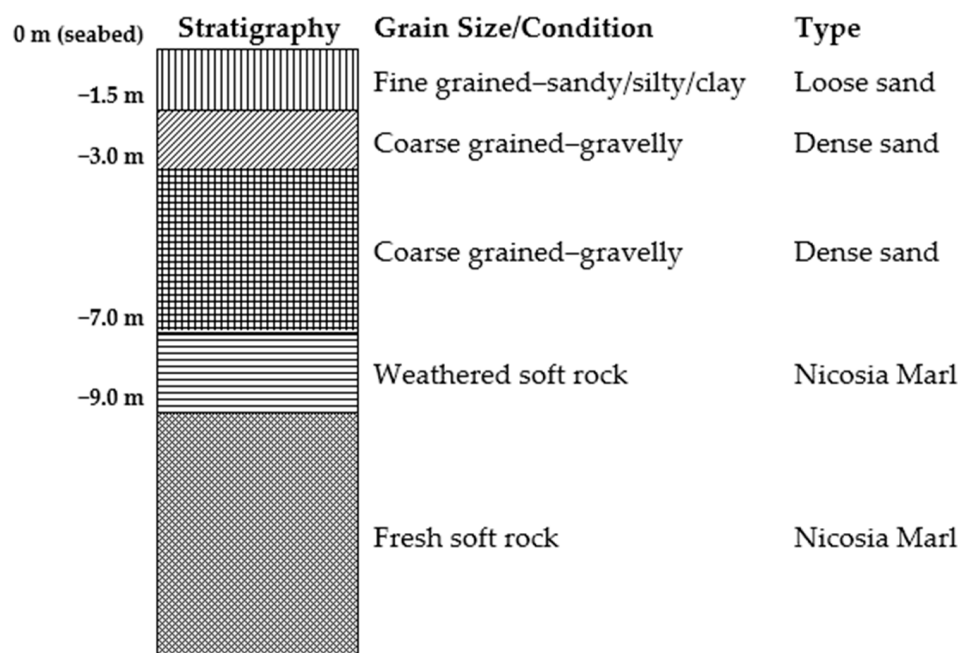

Figure 3. Soil stratigraphy with the grain size and characterization.

Below the dense sand layer, Nicosia marl was found, with the first 2 m being weathered, followed by fresh marl. As documented by previous site investigation studies conducted onshore in Cyprus, Nicosia marl is soft rock with similar characteristics to stiff clay [47–50]. Offshore data were also available from another site investigation [44] conducted prior to the construction of the reference jetty in the area of Vasiliko. SPT tests at the aforementioned six boreholes revealed N-SPT values larger than 40, verifying the high stiffness of the material. Additionally, soil classification studies provided a plasticity index of 30% and liquid limit of 55%, collectively indicating high-plasticity clay (CH) according to the classification chart of British standards [51].

Unconfined compressive strength (UCS) tests were carried out on samples retrieved from various depths from the six boreholes. The resulting lab data did not indicate any correlation between UCS values and depth, nor did they differentiate between weathered and fresh marl. The UCS values exhibit considerable variability, ranging from 840 kPa to 1545 kPa. The mean and median Unconfined Compressive Strength (UCS) values were calculated to be 1180 kPa and 1170 kPa, respectively, with a standard deviation of 233 kPa. In the absence of more precise data, the mean UCS is considered representative of the material's strength, from which an undrained shear strength (Su) of 590 kPa can be inferred (Su = UCS/2). This Su value is assumed hereafter.

Various relationships correlate the UCS of rock with the small strain Young's modulus (Esi), but none are specifically suitable for Nicosia marl. Existing studies [52,53] propose correlations calibrated against data for claystone, which can be considered a comparable rock type to Nicosia marl due to their similar clayey nature. Applying the correlations proposed by the above studies resulted in Esi values that are larger than expected for the softness of Nicosia marl, rendering them not reliable.

Reese et al. [21] proposed that for stiff clays, Esi can be expressed as follows:

$$Esi = k \times H \tag{1}$$

where H is the depth and k is a parameter that is a function of Su. For Su = 590 kPa, the referred study proposes k = 2000 kN/m^3.

More recently, Loukidis et al. [50] calculated the stiffness of Nicosia marl as a function of effective vertical stress (σ'_v) according to the power of law:

$$Esi = A \times {\sigma'_v}^n \times p_a^{1-n} \tag{2}$$

where p_a is the atmospheric pressure equal to 100 kPa, while A and n are dimensionless parameters. The referred authors calibrated these parameters against lab data for Nicosia marl and proposed $A = 395$ and $n = 0.2$.

Using Equations (1) and (2), the Esi values for the marl layers are estimated and presented in Figure 4. Based on these estimates, the Esi profile assumed for the purpose of this study was determined and its variation with depth is shown in the same figure. The weathered layer of marl is attributed to a smaller small strain stiffness than the underlying fresh marl.
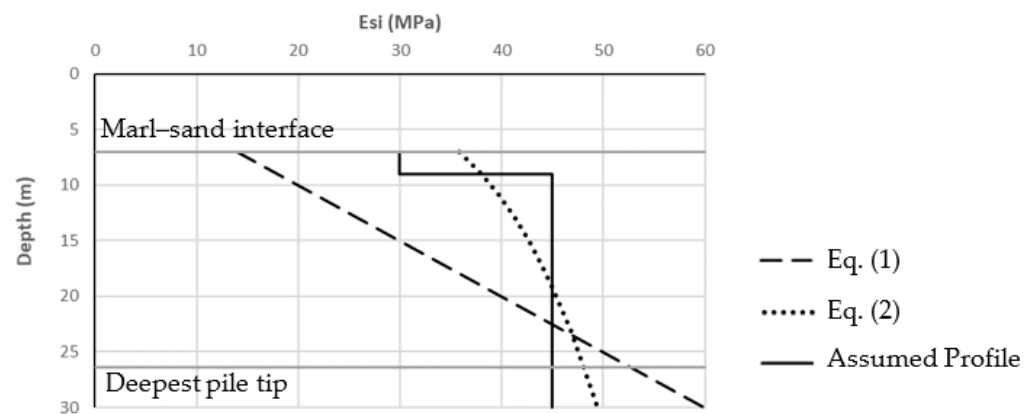

Figure 4. Small strain Young's modulus profile inferred from Equation (1) proposed by [21] and Equation (2) as recommended by [50], superimposed by the assumed profile.

4. Numerical Model

All numerical analyses were conducted using the commercial finite element (FE) software ABAQUS/Standard (2020) [54]. The analyses include simulations of static pushover loading on two marine structures. The first structure is a T-junction of a jetty, as described in Section 2. The second structure is a simplified version of the above, a marine structure with dimensions 8 m × 8 m in plan supported by four piles, conceptualized to facilitate the investigation and decomposition of the mechanisms of resistance to the base moment and shear. The pushover simulations aim to establish the capacity of the examined SPSI systems for lateral loading, which is the main loading condition for such marine structures. These simulations were carried out under various assumptions regarding the soil–pile interaction and steel nonlinearity. Given the flexibility of these structures and the expected large displacements, all analyses accounted for geometric nonlinearity.

The SPSI^{jetty} model simulate explicitly the T-junction of the jetty described in Section 2. As Figure 5 illustrates, the model consists of a 1.3 thick deck and 24 inclined piles with

geometrical characteristics identical to the ones shown in Figure 2. The deck is free to move laterally, neglecting the impact of the trestles that attach at the three sides of the deck. Figure 6 presents the $SPSI^{8 \times 8}$ model that simulates the 8×8 marine structure supported by four piles. The piles have an identical cross-section and length to piles of the T-junction (see Figure 2), thus reaching a depth of 26.35 m. Similarly, the deck thickness and elevation above sea level, as well as site conditions, are the same for the two examined structures.
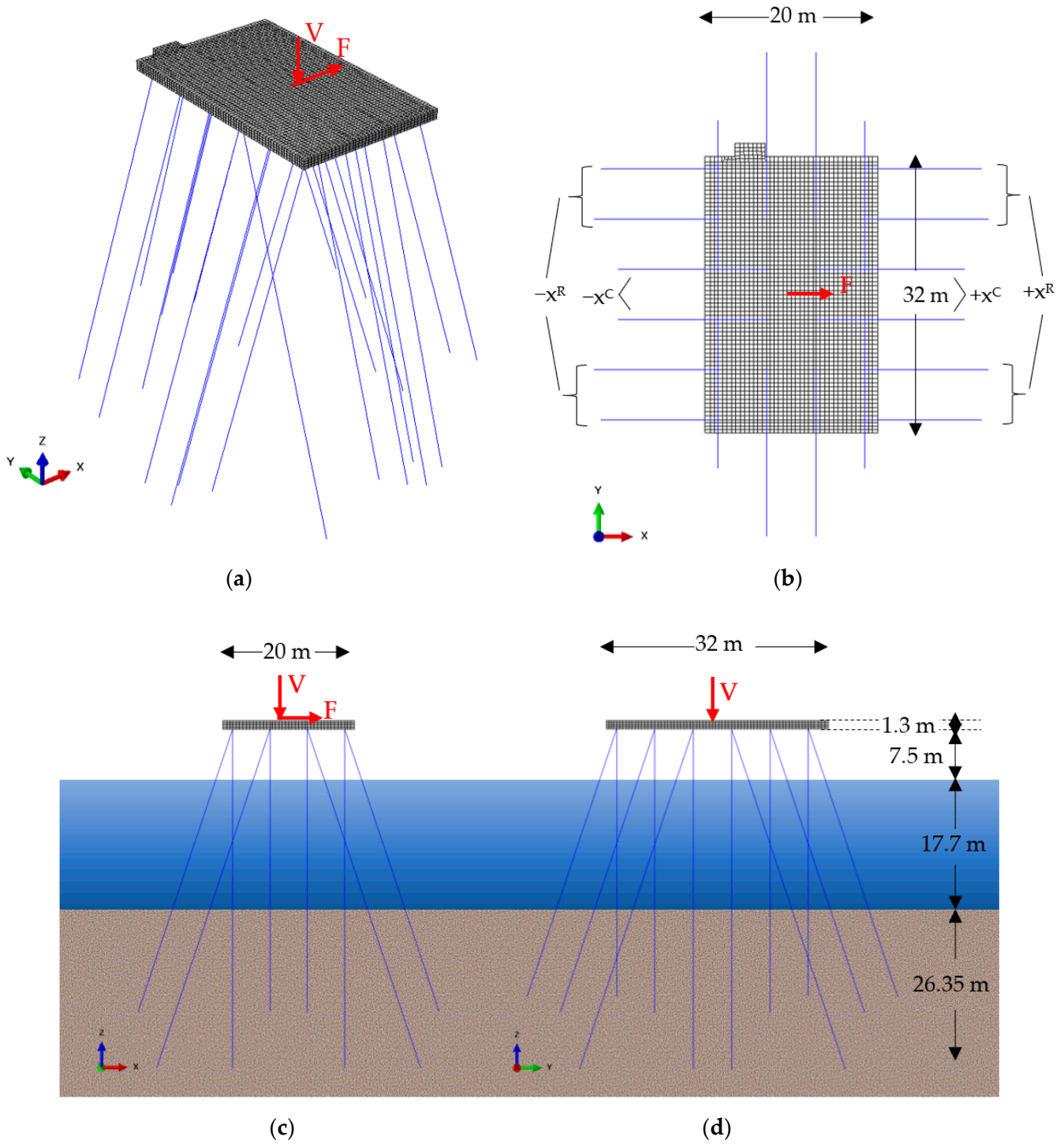
Figure 5. FE structural model of the $SPSI^{jetty}$ system in (**a**) isoparametric, (**b**) plan (x-y), (**c**) x-z side, and (**d**) y-z side views.
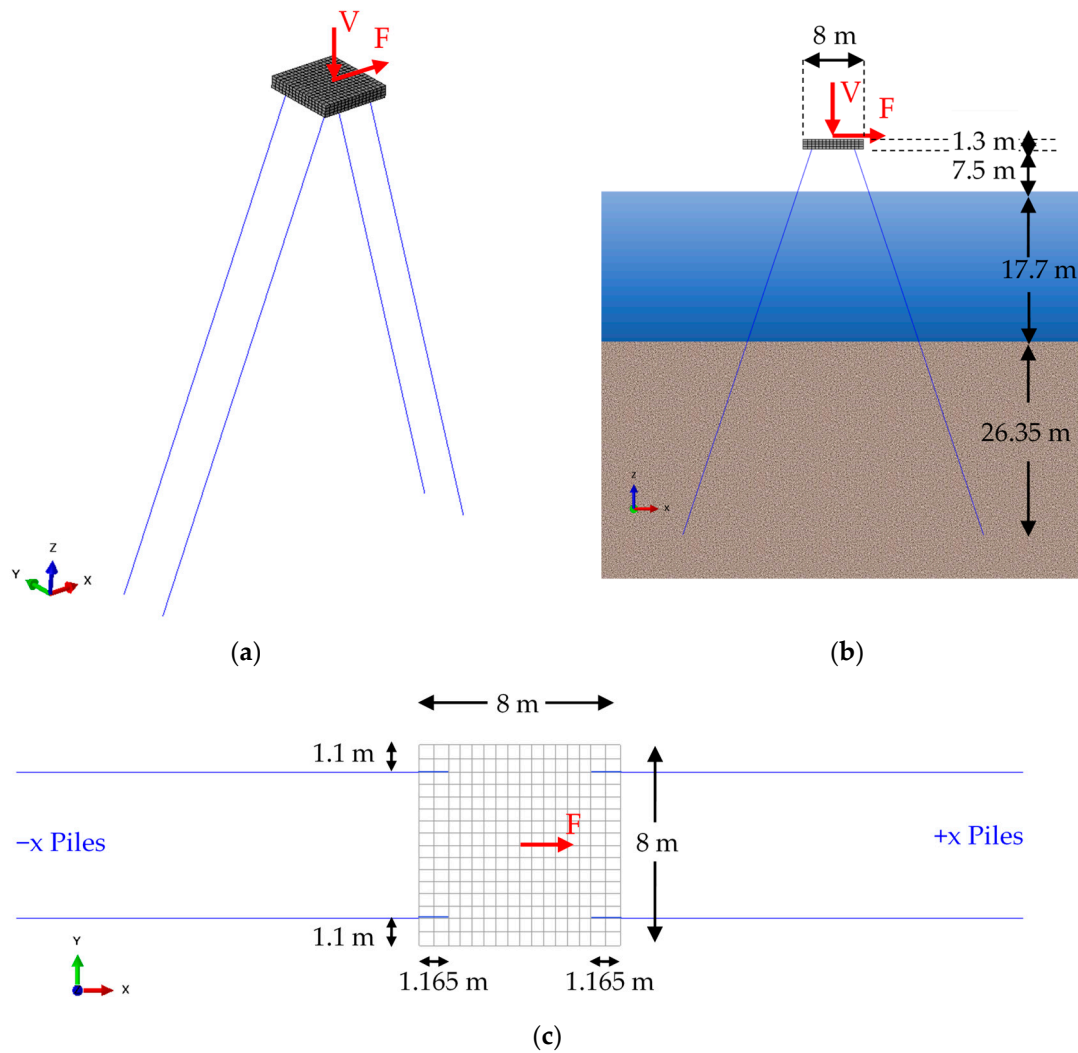
Figure 6. FE structural models of the SPSI$^{8\times8}$ system in (**a**) isoparametric, (**b**) x-z side, and (**c**) plan (x-y) views.

4.1. Structural Elements

The deck and piles of the two modelled marine structures share the same mesh discretization and properties. The concrete slab was simulated using 20-node quadratic brick elements with reduced integration (C3D20R), with approximate dimensions of 0.5 m in the x and y directions and 0.325 m in the z direction. The concrete was assumed to behave elastically, as negligible bending is anticipated.

For the piles, 3-node quadratic beam elements (B32) of approximately 0.50 m in length were used. Each pile comprises two different materials: the first 2.4 m, where the concrete plug is present, is prescribed to be significantly stiffer than the remaining pile, which is hollow and made of plain steel. Due to its higher stiffness, the former pile segment is assumed to behave elastically, whereas the plain steel segment is modelled either as elastic (ELsteel) or elastoplastic (EPsteel). For EPsteel, beam elements are assigned to a plastic mechanical behaviour, assuming that a strain hardening behaviour of 10% strain at failure (ε_u) is prescribed for the steel. The stress–strain behaviour is computed according to Ramberg and Osgood [55] to ensure a smooth elastic–plastic transition and corrected to true stress–strain relationships, following ABAQUS guidelines. Table 1 presents the plastic properties adopted for the steel piles, while Figure 7 presents the associated stress–strain curves incorporated into the analyses.

Table 1. Adopted steel properties.

Acronym	Behaviour	f_y (MPa)	f_u (MPa)	ε_u (%)
ELsteel	Elastic	n/a	n/a	n/a
EPsteel	Elastoplastic	450	550	10
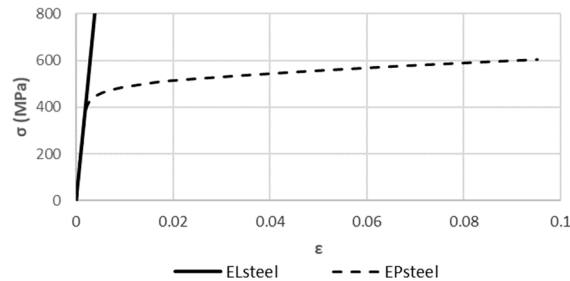
Figure 7. Stress–strain curves incorporated in the analyses to prescribe steel behaviour.

Aiming to simulate the moment connection between the beam elements of the piles and the brick elements of concrete deck, the beam elements are extended and embedded into the brick elements. As discussed by previous studies [56–58], this approach is adequate when the individual beam elements are not subjected to torsion. Additionally, as has been shown by the same studies, the moment capacity of the beam–brick element connection is a function of the stiffness of the embedded beam. Herein, rigid embedded beam elements are used to simulate rigid connections. These elements are positioned vertically to ensure common displacement nodes with the host brick elements and have a length equal to the vertical length (z-direction) of two brick elements. Table 2 summarizes all elastic properties adopted herein for the structural elements.

Table 2. Adopted elastic properties of structural elements.

Material	E (GPa)	ρ (Mg/m^3)	ν
Concrete	34	2.5	0.2
Steel–concrete plug composite	297	55.38	0.3
Steel	210	7.85	0.3
Rigid extension	2×10^6	0.01	0.3

The SPSI^{jetty} numerical model consists of a total of 57,750 nodes, 10,852 brick elements, 2248 beam elements of finite stiffness, 48 rigid beam elements, and 5662 spring elements (see Section 4.2). The smaller model, SPSI$^{8\times8}$, consists of a total of 6645 nodes, 1024 brick elements, 432 beam elements of finite stiffness, 8 rigid beam elements, and 1280 spring elements (see Section 4.2). Preliminary sensitivity analyses were carried out for both models and indicated the adequacy of the adopted element sizes, with negligible size effects observed.

4.2. Soil–Pile Interaction

The soil–pile interaction is considered by the action of T-z and P-y springs positioned at all nodes of piles below the seabed level and the action Q-z springs used at the end nodes of piles. Two P-y springs were used for each buried pile node, acting in the x and y directions of the model, with reference the coordinate systems shown in Figures 5 and 6. These springs aim to simulate the lateral resistance of soil, while T-z and Q-z springs, which act in the z-direction of the model, aim to simulate the shaft and base resistance of piles, respectively. All springs are prescribed to behave either linearly or nonlinearly, while for simplicity, their constitutive behaviours neglect detachment or sliding between the piles and the soil.

Existing stress–strain relationships expressing the soil resistance are typically distinguished based on whether the loading is static or cyclic. This study applies a static incremental lateral force; hence, the corresponding relationships are utilized. Additionally, soil resistance is typically a function of the soil type, with the established relationships that exist in the literature differentiating between sand and clay soils. In this study, the spring behaviour simulating the soil–pile interaction within the first 7 m, where sand layers are present, is determined using existing relationships derived from sand data. For the remaining springs, which simulate the marl–pile interaction, the spring behaviour is determined based on relationships derived from clay data, considering that marl behaves similarly to stiff clay [47–50].

4.2.1. Nonlinear Springs

The nonlinear axial force–vertical displacement behaviours of T-z and Q-z springs were inferred from the corresponding subgrade reactions, τ-z and q-z, determined following the recommendations from API [39]. The recommended τ-z and q-z curves are provided in Figure 8. According to these recommendations, nonlinear τ-z and q-z reactions depend on the critical displacements, z_c, at which the shaft and base resistances are fully mobilized, as well as the ultimate shaft (τ_{ult}) and ultimate base (q_{ult}) resistances. In the absence of related site investigation data, z_c is taken equal to 1% of the pile diameter (D) for both shaft and base resistances. The recommended q-z curves coincide for sand and clay soils, whereas the τ-z curves differ, as a post-peak softening behaviour is suggested for the clay soils (Figure 8a). The residual stress (τ_{res}) is decreased by a factor γ that takes values between 0.7 and 0.9. Herein, γ is taken equal to 0.9.
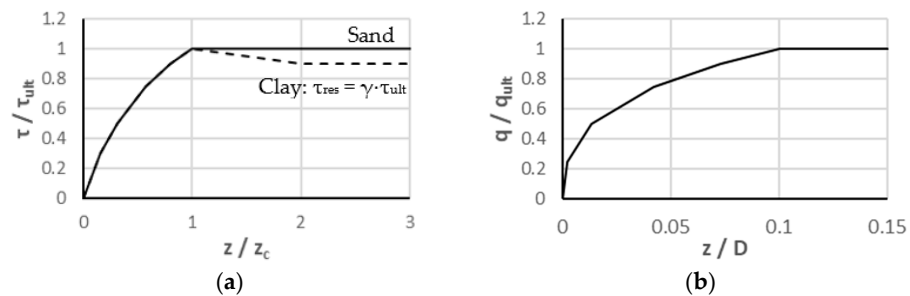

Figure 8. (**a**) τ-z and (**b**) q-z curves recommended by API [39].

In the present study and following the DNV guidelines [40] for piles driven in sand, τ_{ult} is expressed as follows:

$$\tau_{ult} = \beta \times \sigma'_v \tag{3}$$

where σ'_v is the effective overburden pressure and β is a dimensionless shaft friction factor. The β factor is a function of the soil relative density, and for the present study it is taken equal to 0.37 that corresponds to medium dense to dense sand [40].

For piles in cohesive soils, τ_{ult} and q_{ult} can be calculated as follows [39]:

$$\tau_{ult} = \alpha \times Su \tag{4}$$

$$\alpha = 0.5 \times \psi^{-0.5}, \text{ for } \psi \leq 1 \text{ or } \alpha = 0.5 \times \psi^{-0.25}, \text{ for } \psi > 1 \tag{5}$$

$$q_{ult} = 9Su \tag{6}$$

where α and ψ are dimensionless parameters, with $\psi = Su/\sigma'_v$.

For all nonlinear τ-z curves, an identical behaviour was adopted for upward and downward movements of the pile. In contrast, the nonlinear Q-z springs are designed to resist compression only, with zero tensile strength. Aiming to further investigate the impact of the constitutive behaviours of these springs on the SPSI response, in some analyses, Q-z springs were assigned to a tensile strength equal to the compressional one.

For the sand layers up to 7 m depth, the nonlinear force–displacement behaviour of the lateral P-y springs is calculated using Equations (7)–(9) recommended by the guidelines of API [40]. The P*-y (P* expressed in force/pile length units) relationship is a function of the pile diameter (D), initial modulus of a subgrade reaction for lateral loading (k_p) and ultimate capacity in lateral pressure (p_u). The latter, which is a function of σ'_v, is calculated based on modern provisions [39,59], assuming an angle of shearing resistance, φ' equal to 30°. The subgrade reactions were estimated using Equation (9) proposed by Vesic [60]. Parameters required for the calculation of k_p are the soil's small strain Young's modulus (E_{si}) and Poisson's ratio (v), as well as the pile's D, Young's modulus (E_p) and moment of inertia (I_p).

$$P^* = A \times p_u \times \tanh\left(\frac{k_p \times H \times y}{A \times p_u}\right) \tag{7}$$

$$A = (3 - 0.8H/D) \geq 0.9, \text{ for static loading} \tag{8}$$

$$k_p = \frac{0.65 E_{si}}{D(1 - v^2)}\left(\frac{E_{si} D^4}{E_p I_p}\right)^{1/12} \tag{9}$$

API [39] provides guidelines on the lateral stress–displacement, p-y, behaviour of a soft clay–pile interaction, whereas less guidance is provided for stiff clay, which reflects soil conditions for the marl layers. Reese et al. [21] propose specific guidelines to define p-y curves suitable for stiff clay, which are adopted in the present study. Figure 9 presents the proposed curve defined using Equations (10)–(16).

$$p = k \times y \tag{10}$$

$$p = 0.5 \times p_c \times (y/y_c)^{0.5} \tag{11}$$

$$p = 0.5 \times p_c \cdot (y/y_c)^{0.5} - 0.055 \times p_c \times \left(\frac{y - A'y_c}{A'y_c}\right)^{1.25} \tag{12}$$

$$p = 0.5 \times p_c \times (6A')^{0.5} - 0.411 \times p_c - 0.0625 \times p_c \times \frac{y - 6A'y_c}{y_c} \tag{13}$$

$$p = 0.5 \times p_c \times (6A')^{0.5} - 0.411 \times p_c - 0.75 \times p_c \times A' \tag{14}$$

$$p_c = \min\{2 \times Su \times D + \gamma' \times DH + 2.83 \times Su \times H, 11 \times Su \times D\} \tag{15}$$

$$y_c = \varepsilon_c \times D \tag{16}$$

where A' is an empirical adjustment factor for static loading, p_c is the ultimate resistance, ε_c is a strain corresponding to a stress of 50% of the ultimate stress, γ' is the effective unit weight of soil, and H is the depth. Following the recommendations of the referred study, [21], $A' = 0.3$, k = 2000 kN/m^3 (as justified in Section 2), and $\varepsilon_c = 0.004$.
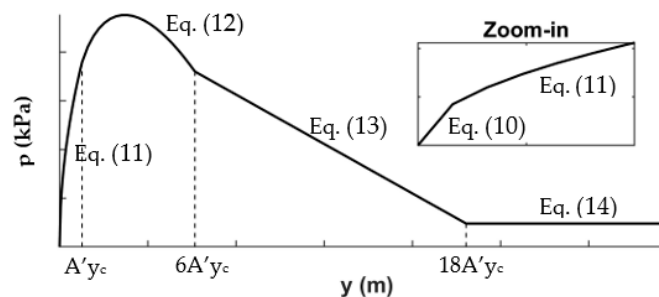

Figure 9. Adopted reference p-y curve (drawn using the equations proposed by Reese et al. [21]).

Tables 3 and 4 present the soil and structural properties, respectively, input in the above equations to define the behaviours of all spring sets. As shown in Table 3, the first 1.5 m of soil is disregarded as the site investigation indicated loose sand of very low

stiffness susceptible to scouring. The properties of the remaining layers were based on outcomes of the site investigation and lab experiments, as described in Section 2.

Table 3. Soil properties adopted for the calculation of the behaviours of the springs.

Layer No	Soil Type	Depth below the Seabed (m)	γ (kN/m^3)	E_{si} (MPa)	ν	φ' (°)	Su (kPa)
1	Loose sand	0–1.5			Disregarded		
2	Dense sand	1.5–3.0	19.4	60	0.3	30	-
3	Dense sand	3.0–7.0	19.4	100	0.35	30	-
4	Weathered Nicosia marl	7.0–9.0	20.6	30	0.35	-	590
5	Fresh Nicosia marl	9.0–26.35 (deepest pile tip)	20.6	45	0.35	-	590

Table 4. Structural properties adopted for the calculation of the behaviours of the springs.

D (m)	E_p (MPa)	I_p (m^4)
1.067	2.10×10^5	1.19×10^{-2}

It is evident from the above that spring behaviour is depth-dependent. However, for simplicity, the soil–pile interaction within each layer is represented by a series of springs with the same force–displacement behaviour. For each layer, this behaviour is computed by following the above procedure and assuming the mid-depth of the layer. For the fresh marl layer, the utilized depth is the one between the weather marl–fresh marl interface and the pile tip. For the case of the SPSI^{jetty} model, where piles of three different lengths were driven to different depths, three distinct force–displacement behaviours are employed, each corresponding to the springs of the respective pile.

Following the above process, τ-z and q-z for both sand and marl layers and p-y for the marl layer are determined, with τ, q, and p being expressed in stress units. In order to convert them to force units, τ is multiplied by the pile perimeter and spacing between springs, p is multiplied by the pile diameter and the spacing, while q is multiplied by the close area of pile end. This approach assumes that piles became plugged during driving, which is reasonable for driving piles in stiff cohesive materials [40]. Finally, the P*-y curves defined for the sand layer are converted to force units by multiplying P*, which is expressed in force/pile length units, by the spring spacing.

4.2.2. Linear Springs

The stiffness of the linear T-z (K_T) and Q-z (K_Q) springs is inferred from the initial slope of the nonlinear springs. The stiffness of the P-y springs, K_P, is inferred through the subgrade reaction, k_p, defined by Equation (9) proposed by Vesic [60], as described earlier. This spring stiffness is calculated by multiplying the above reactions by the pile diameter and spacing between nodes. Table 5 provides the computed stiffness of the linear springs.

Table 5. Stiffnesses of linear springs.

Layer No	Soil Type	Depth below the Seabed (m)	K_T (kN/m)	K_Q (kN/m)	K_P (kN/m)
1	Loose sand	0–1.5		Disregarded	
2	Dense sand	1.5–3.0	344.5	-	9626.6
3	Dense sand	3.0–7.0	795.3	-	14,881.9
4	Weathered Nicosia marl	7.0–9.0	9373.2	-	4487.1
5	Fresh Nicosia marl	9.0–11.0	10,000.1	-	6961.9
		11.0–15.35 (pile tip) *	9675.5	556,235.7	6235.0
		11.0–17.85 (pile tip) *	10,217.4	556,235.7	6181.9
		11.0–26.35 (pile tip)	10,858.4	556,235.7	5937.0

* Used for the SPSI^{jetty} model only, which had piles of three different lengths.

4.3. Loading

For both marine structures under examination, SPSI$^{8\times8}$ and SPSI^{jetty}, the external loads consist of a vertical load (V) and a horizontal load (Fx). For simplicity and exploiting the rigidity of the slab, both loads are applied statically as point loads at the centre of the deck, as illustrated in Figures 5 and 6. The vertical load, with magnitudes of 3.9 MN for SPSI$^{8\times8}$ and 39 MN for SPSI^{jetty}, represents the dead and live loads and it is applied incrementally prior to the application of the horizontal one. The static horizontal load intends to simulate simplistically the dynamic lateral forces resulting from wind, waves, current, or earthquakes, as well as lateral loads from the adjacent trestles. It is applied incrementally until the examined marine structures reach their capacity for lateral loading or the horizontal load reaches a magnitude of 50 MN.

4.4. Sequential Numerical Analyses, Interpretation Approach, and Validation

This study conducts parametric analyses with varied assumptions regarding nonlinearities. The aim of these analyses is to decompose the contributions of the lateral, shaft, and base soil resistances and to emphasize the importance of the associated nonlinear mechanisms, as well as steel plasticity. The approach involves systematically incorporating one nonlinear mechanism per analysis for each of the two examined systems (SPSI$^{8\times8}$, SPSI^{jetty}) separately. The first analysis is linear elastic, while the second one incorporates nonlinear shaft soil resistance. Subsequently, the nonlinearity of the base resistance is added to a third analysis, while the fourth analysis accounts for the nonlinear behaviour of all shaft, base, and lateral soil resistances. Finally, steel plasticity is incorporated. A systematic comparison between analyses is presented to highlight the importance of each nonlinear mechanism in the response.

The response is evaluated through applied force and resultant displacements curves. The stiffness of the response is assessed through the slope of the force–displacement curves, while the system's capacity is indicated by a plateau in the same curve. Additionally, the springs reactions are analysed to demonstrate the contributions of the three resistance mechanisms to the base shear and moment.

In the absence of field data, which would have provided a more rigorous validation, the numerical models were validated based on equilibrium checks. In particular, the lateral reactions were compared with the applied vertical load, and the sum of spring reactions acting in the (lateral) x-direction was compared with the applied horizontal load. Finally, the numerical results were compared with the design study, showing reasonable agreement for the analyses conducted with boundary conditions and inputs that align with the design study.

5. Results

5.1. SPSI$^{8\times8}$ Marine Structure

Soil nonlinearity in this study is accounted for using springs with nonlinear force–displacement behaviour. The effect of these nonlinear springs on the response of the SPSI$^{8\times8}$ marine structure is demonstrated in Figure 10. The figure presents the applied horizontal force, Fx, and the resulting horizontal displacements (x-direction), d, at the centre of the deck. As expected, incorporating spring nonlinearity reduces the system's stiffness, as shown by the decreased slope of the Fx-d lines, and increases the resulting displacements. Specifically, when nonlinearity is applied only to T-z springs, the system becomes more flexible compared to the fully linear system, while maintaining constant stiffness once the T-z springs approach their capacity (i.e., shaft resistance is fully mobilized). However, when nonlinear Q-z springs are included, the analysis stops abruptly without reaching a plateau, indicating brittle failure. A similar pattern is observed with nonlinear P-y springs, though there is a slight additional decrease in stiffness.
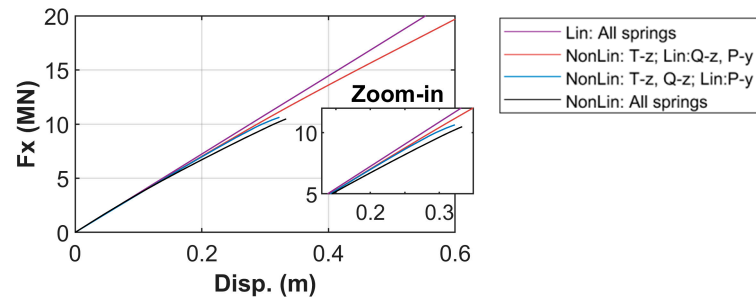
Figure 10. Impact of spring nonlinearity on the response of the $SPSI^{8\times8}$ marine structure.

The above discussion indicates that the constant stiffness during full mobilization of shaft resistance in a system with nonlinear T-z springs but linear Q-z and P-y springs is upheld by the linear behaviour of the latter springs, especially the Q-z springs. These springs allow further axial resistance to develop by the soil–pile system after shaft resistance mobilization. The role of the Q-z springs in the axial behaviour of the piles is better explained in Figure 11, which presents the sum of spring reaction forces at the shaft (T), base (Q), and lateral direction (P) when all springs behave nonlinearly. The forces are plotted separately for the −x and +x piles, the positions of which are shown in Figure 6c. The presented accumulation of T, Q, and P forces with increasing deck displacement is superimposed by the maximum and minimum magnitudes possible (thresholds), calculated as the sum of the maximum possible reaction forces of all springs in the model. For the P-z springs that exhibit a softening behaviour after peak, the post-peak residual force is used for the calculation of the thresholds. As the accumulated forces approach the maximum and minimum thresholds, the springs exhibit nonlinear behaviour. They become completely plastic once these thresholds are reached.
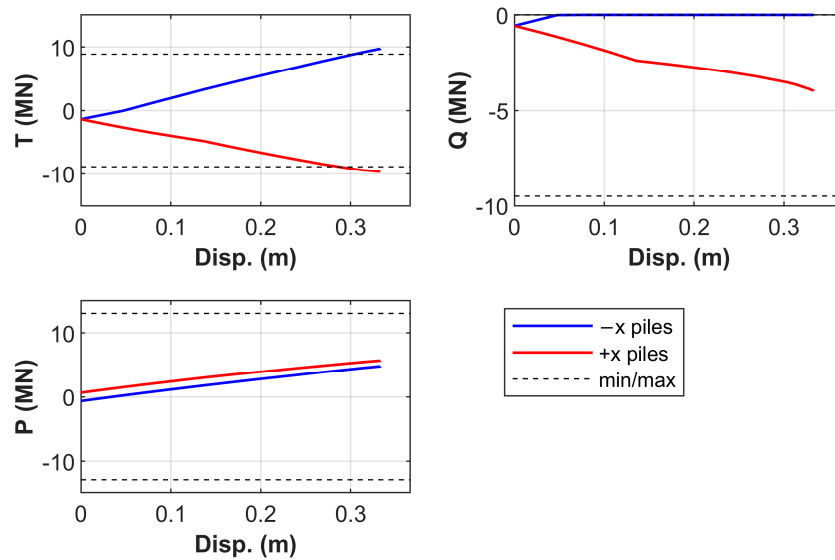

Figure 11. Sum of T, Q, and P forces computed by the analysis with all springs behaving nonlinearly, superimposed by the maximum possible forces.

During loading, the −x piles tend to move upward, while the +x piles tend to move downward. This explains the accumulation of positive (tensile) T and Q reaction forces by the springs of the −x piles and negative (compressive) ones by the springs of the +x piles. As Figure 11 shows, T forces of both −x and +x piles increase linearly until reaching the capacity of the shaft friction. On the other hand, the compressive capacity of the base is not reached, while the tensile capacity is reached very early in the analysis, due to the assumption of zero tensile strength by the base resistance. Finally, the capacity of the P-y curves is not reached at any time during the analysis, indicating that the failure in this case

was related to piles' axial behaviours. The capacity of the system reaches when both the shaft and the base (tensile) resistances of the $-x$ piles reach their capacity. Under the latter condition, the system becomes unstable as vertical equilibrium cannot be ensured, which explains the brittle failure of the system.

The above investigation illustrated the weak influence of the constitutive behaviour of the P-y curves on the $\text{SPSI}^{8\times8}$ system response. To further investigate their role, exaggerated analyses without incorporating P-y springs distributed along the piles are carried out. To ensure analysis stability, linear P-y springs are placed at the three deepest nodes of the four piles. It is noted that similar results would have been achieved if fixity in the x-direction of pile ends was considered; however, springs are preferred to incorporate model compliance in the lateral directions at pile ends. As Figure 12 illustrates, the system without P-y springs has a significantly lower small strain lateral stiffness and lateral load capacity, and a more ductile behaviour compared to the system with P-y springs.
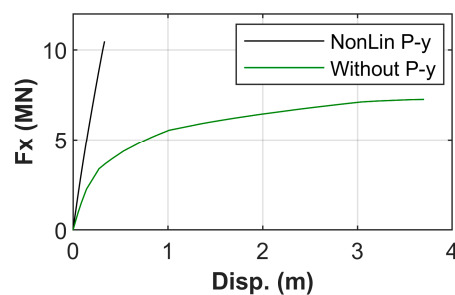
Figure 12. Impact of the absence of P-y springs on the response of the $\text{SPSI}^{8\times8}$ marine structure.

An explanation of this behaviour is provided in Figure 13, which presents the accumulation of total T, Q, and P forces against deck displacements for the analysis without P-y springs. Concerning P forces, these develop to maintain equilibrium in the x-direction, while they have zero impact on the moment equilibrium. With respect to Q forces and as opposed to the case where P-y springs were present (refer to Figure 11), the capacity of the base resistance from the compressional piles (+x Piles) is reached. Prior to this point, both $-x$ and $+x$ piles were generating positive incremental shaft resistance forces, while beyond it, the $+x$ piles begun producing compressional incremental shaft resistance. This trend persisted until failure. At failure, the capacity of the shaft resistance of the compressional (+x) piles was not reached (Figure 13), unlike the case with P-y springs (see Figure 11). Failure occurred due to the system's incapacity to sustain vertical equilibrium after both the shaft and base resistances of the $-x$ piles were reached.

The failure mode observed in the system without P-y springs aligns with the earlier observation from the analysis with P-y springs, reinforcing the predominant influence of axial pile behaviour on the response. However, the investigation also underscores the critical contribution of the P-y springs along the piles to the response of the marine structure under examination. Their absence would result in an erroneous distribution of the spring forces, consequently leading to the wrong prediction of forces and bending moments acting on the piles.

All previous analyses assumed elastic steel; however, steel plasticity is anticipated to influence the response when structural forces and moments are significant. Figure 14 compares the response of the $\text{SPSI}^{8\times8}$ system when steel plasticity is either considered (EPsteel) or neglected (ELsteel). It is observed that when all springs are prescribed to behave linearly, plasticity is mobilized and plays a significant role as large structural displacements occur. However, when nonlinear springs are utilized, plasticity has a minimal impact on the response. This is explained by the fact that failure takes place before steel plasticity becomes significant. In fact, the first areas of steel yielding occurred at 10 MPa, with failure occurring shortly after (at 10.48 MPa). For EPsteel analyses, similar to the earlier ELsteel analyses, the system's failure is attributed to its inability to sustain a larger vertical load, rather than being directly associated with steel yielding.
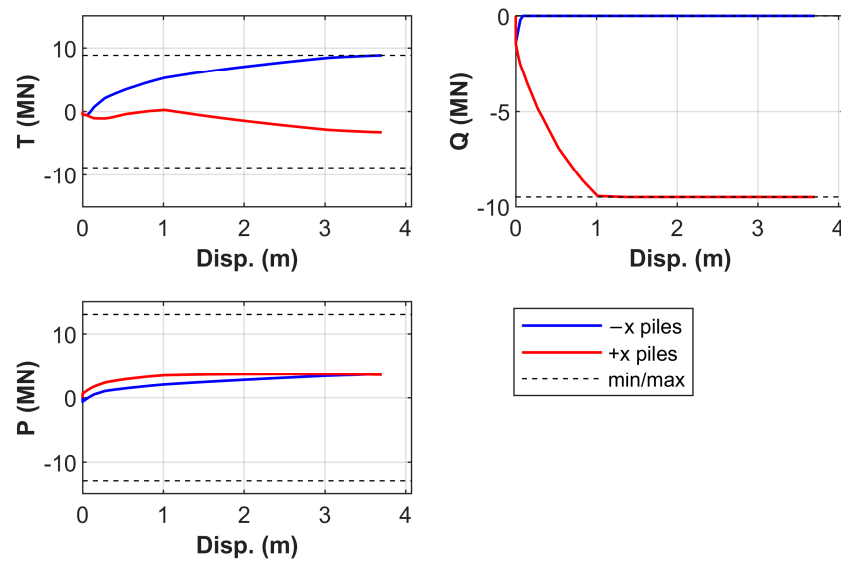
Figure 13. Sum of T, Q, and P forces computed by analyses without P-y springs.
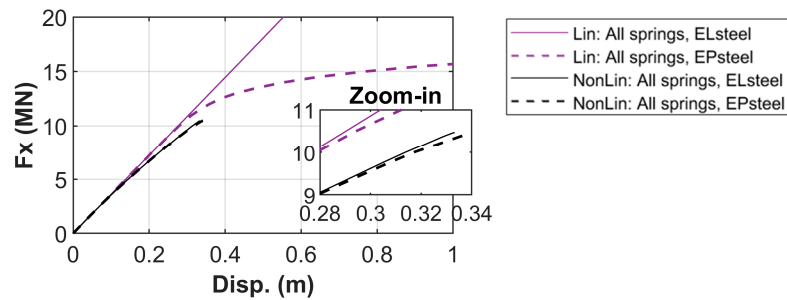

Figure 14. Impact of steel plasticity on the response of the SPSI$^{8\times8}$ system.

The above findings underscore the significance of the axial pile behaviour in the system's response, primarily governed by shaft and base resistances. Aiming to focus on the latter aspect, Figure 15 compares the response of the SPSI$^{8\times8}$ marine structure when base resistance either can or cannot sustain tensile stresses. For the EPsteel analyses presented, T-z and Q-z springs are set to behave nonlinearly, while linear P-y springs are employed to isolate the influence of the nonlinear pile axial behaviour. Figure 15 demonstrates that prescribing the Q-z springs to sustain tensile forces results in a notable increase in the system's lateral load capacity. Simultaneously, the system exhibits greater ductility compared to when tension is not permitted.
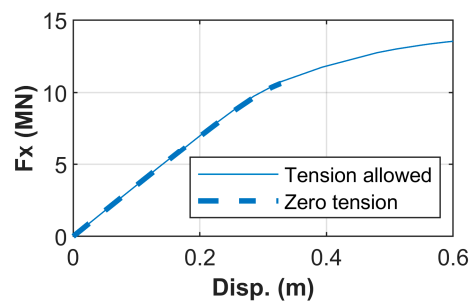

Figure 15. Effect of tension allowance in Q-z springs on the response of the SPSI$^{8\times8}$ system.

Considering the previously discussed failure mode of the analyses with tensionless Q-z springs, the observed increase in the system's capacity when tension-resistant springs are used is attributed to the enhanced axial capacity of the soil–pile interaction. Figure 16, which compares the accumulation of T, Q, and P forces computed by the above two analyses,

provides evidence on the above claim. When Q-z springs can sustain tensile forces, the
$-x$ piles do not reach their capacity as early as the analyses where tension is not allowed.
This increases the axial loading capacity of the $-x$ piles, thereby increasing the lateral
load capacity of the entire marine structure. Additionally, by allowing the $-x$ piles to
develop tensile Q forces, the positive T forces are alleviated compared to when Q-z springs
are tensionless. On the other hand, all springs that act on the +x (compressive) piles
remain unaffected.
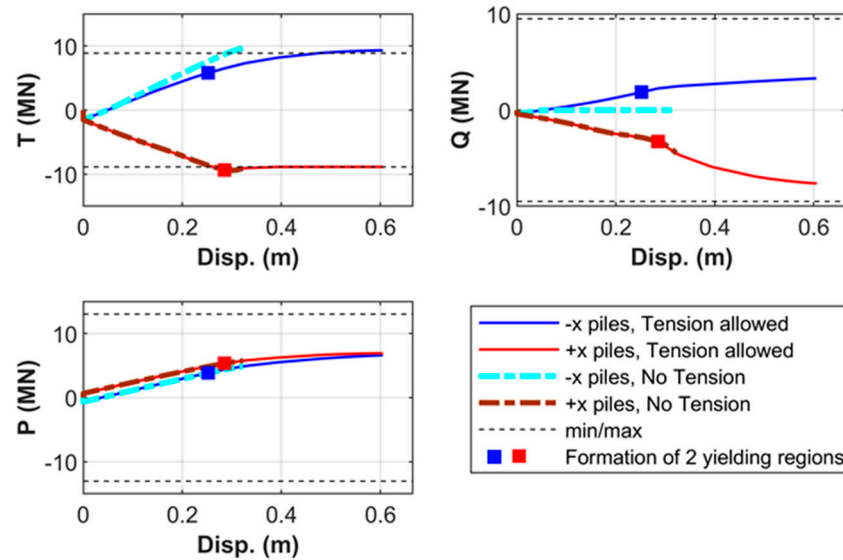
Figure 16. Sum of T, Q, and P forces computed by analyses with and without tension allowance for
the Q-z springs.

The ductile behaviour observed in Figure 15 for the case when tension is allowed,
i.e., stiffness decreases steadily approaching a plateau, can be attributed to structural
nonlinearity. By allowing larger pull-out forces and therefore displacements to take place,
four plastic regions were created at the piles. As illustrated in Figure 16, the first two were
created at $-x$ tensile piles at interface between the elastoplastic plane steel beams with
the elastic and much stiffer composite (refer to Section 4.1). At the following increment,
another two plastic regions are created at the same elevation for the +x compressive piles.
Subsequently, the axial forces (T + Q) of the compressive (+x) piles increases rapidly,
approaching piles' axial bearing capacity, while the tensile axial forces of the $-x$ pile
remaining almost constant.

From the above discussion, it is concluded that by allowing Q-z springs to carry tensile
forces non-conservatively, the anticipated capacity of the system in lateral force will exceed
that if Q-z springs were limited to carrying only compressional forces.

5.2. SPSI^{jetty} Marine Structure

This section discusses the numerical results from pushover simulations conducted on
the jetty model SPSI^{jetty}, which is a representative of the real jetty described in Section 2.
The objective of this investigation is to explore how assumptions regarding springs, which
represent soil compliance, and steel behaviour impact a more complex marine structure.

Aiming to investigate the sensitivity of the small strain lateral stiffness (Kx) of the
SPSI^{jetty} marine structure to the initial stiffness of the springs, linear elastic parametric
analyses were carried out. Figure 17 presents the variation of Kx with the springs' stiffness
(K_{spring}) normalized to the original stiffness of springs ($K_{0,spring}$), which is provided in
Table 5. Each of the presented lines resulted from analyses that vary only one of K_T, K_Q, or
K_P while keeping the original stiffness for the remaining spring sets. Figure 17 indicates
that the model's small strain stiffness is very sensitive to the elastic stiffness of T-z springs.
P-y springs seem to have an influence on Kx when they have very small stiffness, with

weak impact when they are stiff. Finally, Kx is almost insensitive to the elastic stiffness of Q-y springs.
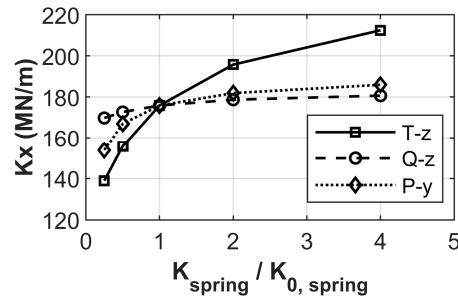
Figure 17. Sensitivity of the linear elastic stiffness of the SPSI^{jetty} marine structure to the stiffness of linear springs.

For larger strain problems, linear elastic analyses are inadequate due to the anticipated nonlinear soil behaviour. Figure 18 presents the input force (Fx)–deck horizontal displacement (d) behaviour output from numerical analyses with various assumptions regarding the behaviour of T-z, Q-z, and P-y springs. As the figure illustrates, and as observed for the smaller SPSI$^{8 \times 8}$ marine structure, when only the T-z springs behave nonlinearly, the SPSI^{jetty} response becomes more flexible but still exhibits linear behaviour. As explained earlier, this is because the overall axial behaviour of the soil–pile interaction is controlled by the linear base springs. The latter also explains the highly nonlinear behaviour of the SPSI^{jetty} when nonlinear Q-z springs are incorporated. When both T-z and Q-z springs behave nonlinearly, then the entire axial behaviour of the soil–pile interaction behaves nonlinearly. Once the axial soil–pile interaction capacity is reached, any increase in base moment due to an additional horizontal load is sustained by the linear P-y springs, resulting in the observed constant, yet smaller, stiffness. When, though, all springs behave nonlinearly, the system exhibits nonlinear behaviour until failure. The impact of the nonlinearity of the P-y springs becomes apparent only when structural displacements are already large (i.e., 1 m lateral deck displacement).
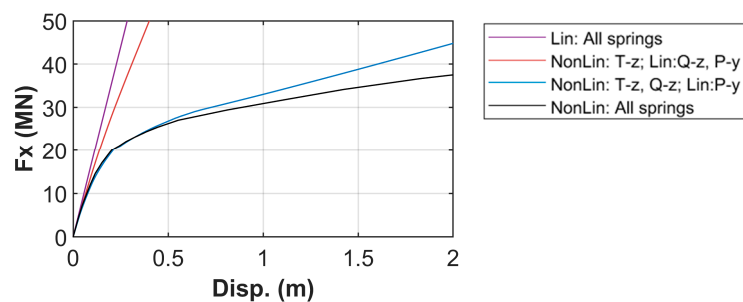
Figure 18. Impact of spring nonlinearity on the response of the SPSI^{jetty} marine structure.

Figure 19 presents the force–force displacement system's behaviour computed by analyses with various assumptions regarding the base springs. It is evident that when these springs are completely absent, the examined system's response is significantly more flexible than systems that incorporate base springs. This can be attributed to the considerably decreased axial capacity of the individual soil–pile interaction systems. As observed for the SPSI$^{8 \times 8}$, the SPSI^{jetty} marine structure exhibits a stiffer response and a higher capacity for lateral loading when Q-z springs can sustain tensile forces, either when these behave linearly or nonlinearly. Particularly, the SPSI^{jetty} system has a very stiff response with slight nonlinearities when Q-z are linear due to the unlimited axial capacity, which highlights further the significant role of the axial behaviour of soil–pile interaction systems.
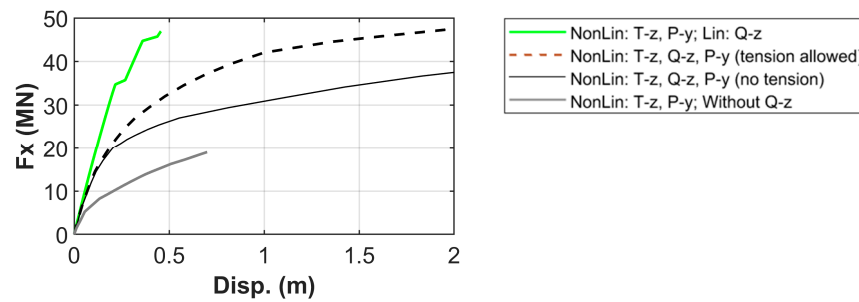
Figure 19. Sensitivity of the lateral response of the SPSI^{jetty} model to the behaviour of Q-z springs (T-z and P-y springs are nonlinear).

Additionally, the imposition of linear Q-z springs, instead of the more reasonable nonlinear springs, affects the reaction spring forces, as illustrated in Figure 20. The figure plots the sum of T, Q, and P reaction forces acting on the centre (C) or rear (R) piles that are placed either at the negative ($-$x) or positive ($+$x) axis of the model. With reference Figure 5, $-$x^C and $-$x^R piles are expected to develop tensile incremental forces (i.e., tend to move upwards), whereas $+$x^C and $+$x^R piles are expected to develop compressional forces (i.e., tend to move downwards). Figure 20 compares results from analyses with either linear or nonlinear tensionless Q-z springs. As expected, for the linear Q-z spring scenario, larger Q forces are developed. More importantly, it is demonstrated that when linear Q-z springs are used, the resulting T forces are significantly smaller for all springs than the forces resulting from the analysis with nonlinear Q-z springs. With respect to P forces, the Q-z springs' constitutive behaviour seems not to affect the forces acting on the tensile, $-$x, piles. However, the use of linear springs significantly increases the resultant P forces of the $+$x^C piles and decreases (up to a certain force limit) those acting on the $+$x^R piles. The implication of this is that the springs of the $+$x^C piles develop such large forces that they reach the peak force, which is then followed by the softening behaviour illustrated in Figure 9. This softening behaviour can justify the abrupt decrease in P forces on the $+$x^C piles (when Fx = 35 MPa). Once the softening stage is reached, the demand on the lateral load resistance is sustained by the increase in spring reactions of the $+$x^R piles, as evidenced by the horizontal step to larger P values observed Figure 20.

The impact of these steps, which indicate rapid changes in the P conditions, on the response is illustrated in Figure 21. The figure presents results from the analyses with linear Q-z springs, specifically superimposing the force–displacement response of the SPSI^{jetty} model with the total P reaction forces of the in-plane $-$x (i.e., both $-$x^C and $-$x^R) and $+$x (i.e., both $+$x^C and $+$x^R) piles. By combining Figure 21 with Figure 20, it becomes apparent that the horizontal steps observed on the P forces of the $-$x and $+$x piles shown in the former figure are associated with the steps observed on the $+$x^C and $+$x^R piles shown in the latter figure. These rapid changes in the P forces also influence the force–displacement response of the system, as evidenced by similar steps in the response shown in Figure 21.

While the above discussion indicates an almost linear response of the system when linear Q-z springs are used (Figure 19), this would not occur if plastic regions were allowed to form on the piles. Instead, steel plasticity could decrease the stiffness of the system progressively, leading the force–displacement curves to a plateau, a feature that has not been observed in any ELsteel analyses shown in Figure 19. Within this context, Figure 22 explores the impact of steel plasticity combined with the constitutive behaviour of the Q-z springs, emphasizing tension allowance. As expected, when elastoplastic steel is employed and plasticity is mobilized, a weaker response is observed. EPsteel analyses reached a plateau, indicating that the system's capacity under lateral loading is reached.
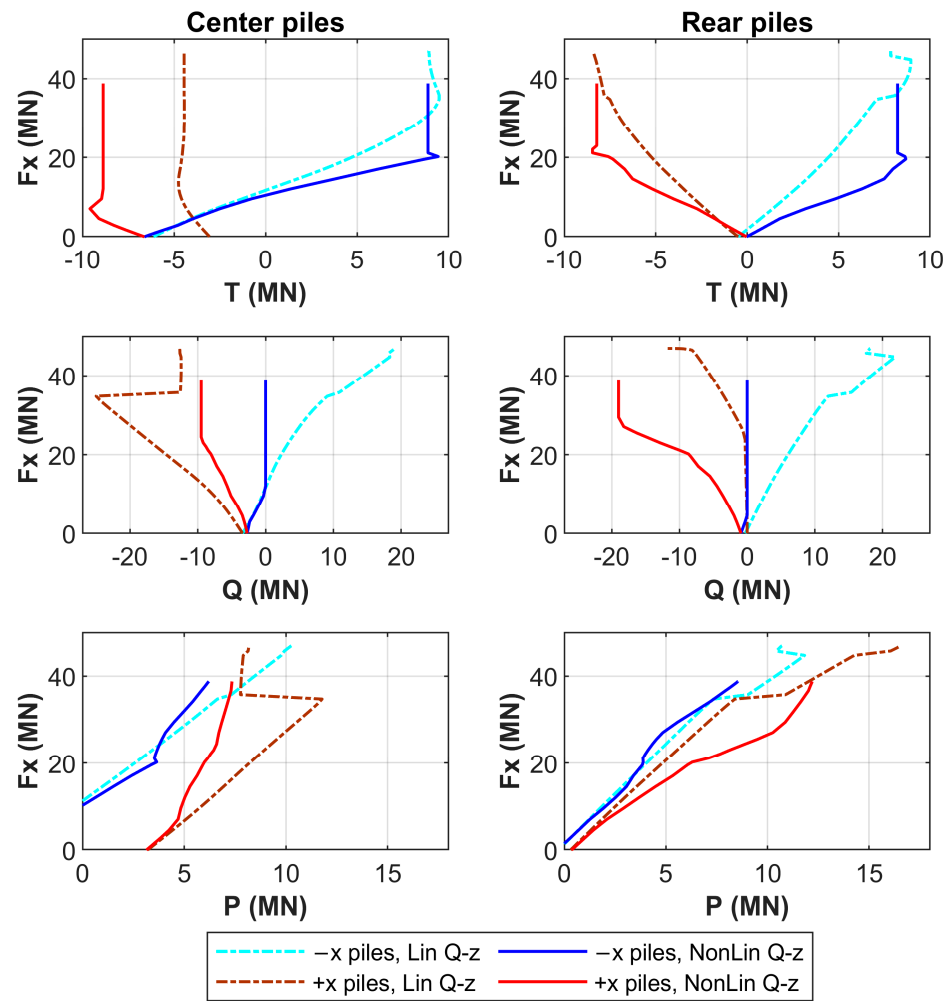
Figure 20. Variations of T, Q, and P forces with the input horizontal force computed by analyses that incorporate either linear or nonlinear Q-z springs.
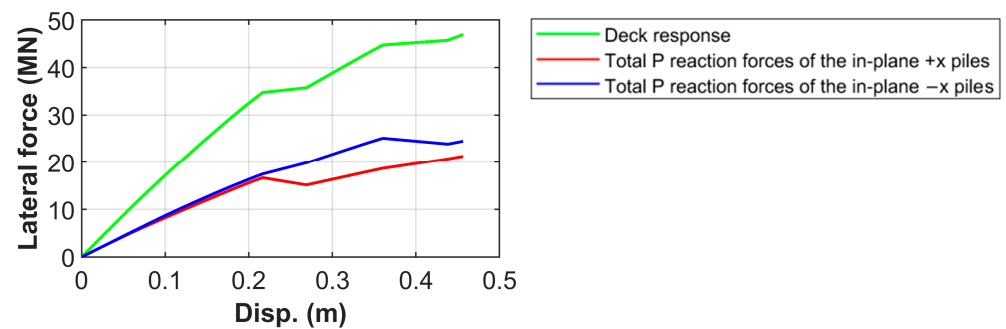

Figure 21. SPSI^{jetty} response and P force accumulation during the analysis with linear Q-z springs. The P forces resulting from the vertical load are removed from the results, isolating the forces accumulated from the lateral load.

As shown in Figure 22, the lateral load and deck displacement that correspond to the first plastic yield (indicated by the deviation between EPsteel and ELsteel results) depend on the assumption made regarding tension allowance. When tension-resistant Q-z springs are used, the consequent stiffer response restricts the displacements and impose larger axial forces and bending moments on the piles. Therefore, under these conditions, the first yield of piles occurs at a larger force but smaller displacement than the ones of a system with tensionless Q-z springs (see Figure 22).
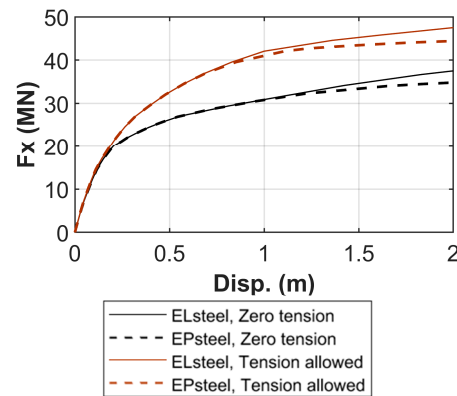
Figure 22. Effects of steel plasticity and the tension allowance of Q-z springs on the SPSI^{jetty} response.

Similarly, forces and displacements corresponding to the first yield is a function of the behaviour of P-y springs, as illustrated in Figure 23. It shows that the imposition of linear springs results in a stiffer response compared to when nonlinear springs are used; thus, plasticity is mobilized on larger forces and smaller displacements. For the case without P-y springs, the capacity of the system is reached, because the axial capacity of the system is fully mobilized. This occurs before any plastic yield forms on the piles, justifying the zero impact of steel plasticity shown in Figure 23.
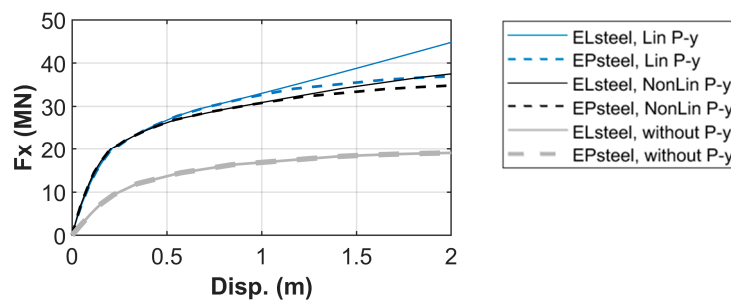

Figure 23. Effects of steel plasticity and the behaviour of P-y springs on the SPSI^{jetty} response.

6. Discussion

The above investigations verify that SPSI phenomena can decrease the base shear and capacity while increasing the displacements of marine structures compared to systems where SPSI is neglected. These observations have been well established in the literature for marine structures [3,10,43], and they are a consequence of the increased flexibility induced by soil compliance and nonlinearity.

Analyses of both SPSI$^{8\times8}$ and SPSI^{jetty} structures demonstrated that the critical resisting mechanism is the axial behaviour of piles. In fact, the systems' capacity for lateral loading is found to be strongly associated with the axial capacity of piles, especially those subjected to tensile loading. The axial capacity of tensile piles can be reached well before the capacity of the compressional piles due to the tensionless behaviour of base resistance. As observed for the SPSI$^{8\times8}$, which has only four piles, when the shaft capacity of the two tensile piles is reached, then the system fails in a brittle manner, due to its incapability to sustain equilibrium in the vertical direction. The same behaviour was not observed on SPSI^{jetty} which is founded on 24 piles, as the axial forces can re-distribute once some piles reach their axial capacity. Nevertheless, both examined marine structures failed due to the axial failure of piles, which contradicts the failure due to structural yielding expected if SPSI was neglected. In agreement with [3], the latter denotes that it can be unconservative to neglect SPSI effects as it can lead to wrong predictions regarding the failure modes, and therefore a wrong prediction regarding the critical elements of marine structures.

Given the established critical role of the axial behaviour of the soil–pile interaction, the present study examined further the base resistance, which is one of the two components consisting this behaviour. Base resistance is sometimes assumed to be capable of sustaining tensile forces, either by prescribing spring stiffness with symmetric behaviour for positive and negative pressures or by assuming full compatibility between the pile and soil elements for the case when the soil is explicitly modelled. This unreasonable assumption is shown to render the examined SPSI systems stiffer and increase their lateral load capacity in an unconservative manner. This is attributed to the fact that tension-resistant q-z springs significantly enhance the tensile capacity of piles, rendering the compressive piles the weakest components. Additionally, the assumption of tension-resistant q-z springs significantly changes the distribution of forces in comparison with those expected when tensionless springs are employed. In particular, for marine structures with a significant number of piles, like the examined SPSI^{jetty} structure, the adoption of such q-z springs can lead p-y forces to increase, substantially approaching their capacity.

While the choice between the linear or nonlinear behaviour of p-y springs was not found to be important for the examined marine structures, their entire omission was shown to lead to a significantly more flexible response and lower capacity system. Omitting p-y springs intensifies the axial loads carried by the piles, causing the system to fail at a lower lateral force due to soil–pile interaction failure. Their absence would lead to an incorrect distribution of spring forces, resulting in inaccurate predictions of the forces and bending moments acting on the piles. In the same manner, it was shown that steel plasticity can be triggered at larger forces and smaller displacements when either p-y or q-z springs are assumed to be linear. Although further investigation is required, the above observations indicate that piles' bending moments and forces depend on the assumptions made on all three spring sets (τ-z, q-z, and p-y). This agrees with conclusions made from pushover analyses by Chigullapally et al. [37], who showed that the magnitude and the location of peak bending moment depend on the ultimate p pressure of the shallow soil. Additionally, a comparison between linear and nonlinear analyses indicates that soil nonlinearity can result in weaker forces and bending moments acting on the structural members, as the system's failure is controlled by soil failure. This observation aligns with the concept of "reversal of capacity design" introduced and implemented by previous studies [61–63]. According to this concept, soil failure can be considered as a means to avoid structural collapse under extreme loading. However, the applicability of this approach on marine structures requires further research and is beyond the scope of the current study.

Whether or not plastic regions are created on piles is a function of the number of piles and the capability of the system to re-distribute the forces after the failure of some piles. A brittle behaviour without any plastic yield was observed for the case of the 4-pile SPSI$^{8×8}$ structure, while a more ductile behaviour was observed for the jetty structure. This is due to the fact that forces re-distribution allowed a further increase in the lateral force and hence the creation of yielding areas on the piles, as well as further progressive yielding of spring elements. This ductile behaviour would have not been observed if SPSI effects were neglected, as was also shown by [3]. Therefore, considering that SPSI phenomena can work positively in increasing a system's ductile behaviour, they facilitate compliance with the demands of provisions for structural design against dynamic (e.g., wave or seismic) loading.

It is noted that the above conclusions are drawn from analyses that account for SPSI effects though the most widely used, yet simplified, approach, which involves springs recommended by the API provisions. To validate these conclusions, experimental field tests and in-field monitoring are required. Additionally, experimental data can account for site-specific conditions in determining soil nonlinearity and the bearing capacity. As documented by previous studies, relying solely on modern provisions for these determinations can be inappropriate under certain circumstances [23,25,28,29,42,64,65]. In-field monitoring and diagnostic inspection of marine structures are essential for ensuring operational safety and effective management. They are also critical before undertaking any

rehabilitation, maintenance, or restoration work on existing structures [65–67]. To this end, an in-field laboratory has been developed at the site of jetty, consisting of accelerometers, weather stations, and wave readers. Some information about this laboratory is provided by Onoufriou et al. [68] and Demetriou et al. [69,70], while its detailed description will be presented in future work.

7. Conclusions

This study presented 3D numerical parametric static pushover analyses of two marine structures, a smaller model with four piles and a larger model representative of a real jetty supported by twenty-four piles. The structures' responses were investigated under the influence of SPSI and assumptions regarding soil behaviour, linear or nonlinear, for the axial and lateral deformation modes. Soil resistance was modelled through p-y, τ-z, and q-z springs, the behaviour of which is prescribed by following API's [39] guidelines, except for the p-y springs associated with stiff clay, for which the formulation proposed by Reese et al. [21] is followed. This study decomposed the contribution of the lateral, shaft, and base soil resistances to emphasize the importance of the associated nonlinear mechanisms, as well as steel plasticity. This was achieved through an approach that systematically incorporated one nonlinear mechanism per analysis for each of the two examined systems ($SPSI^{8\times8}$ and $SPSI^{jetty}$).

The results indicated the critical role of the axial pile–soil interaction behaviour for both structures. The primary failure mechanism for the examined structures was found to be piles reaching their axial capacity, with the lateral soil resistance and structural yielding being less significant. The importance of the latter two components was found to be a function of the assumption made regarding the representation of soil. Additionally, structural yielding can depend on the number of piles and the ability of the system to re-distribute piles' forces and moments after the failure of a component (e.g., axial behaviour of an individual soil–pile interaction system). This ability allows also marine systems to exhibit a ductile response, which is a fundamental requirement for designing against seismic or wave loading. Nonlinear SPSI phenomena can further promote ductile behaviour, as demonstrated herein. Finally, this study highlights the unconservative influence of neglecting these phenomena, as well as considering tension-resistant base (q-z) springs.

Author Contributions: Conceptualization, M.K., T.O. and C.M.; methodology, M.K., T.O. and C.M.; software, M.K.; validation, M.K., T.O. and C.M.; formal analysis, M.K.; investigation, M.K.; resources, M.K., T.O. and C.M.; data curation, M.K.; writing—original draft preparation, M.K.; writing—review and editing, T.O. and C.M.; visualization, M.K.; supervision, T.O. and C.M.; project administration, T.O.; funding acquisition, T.O. All authors have read and agreed to the published version of the manuscript.

Institutional Review Board Statement: Not applicable.

Data Availability Statement: The data presented in this study are available on request from the corresponding author.

Conflicts of Interest: The authors declare no conflicts of interest. The funders had no role in the design of the study; in the collection, analyses, or interpretation of data; in the writing of the manuscript; or in the decision to publish the results.

References

1. van Raaij, K.; Gudmestad, O.T. Wave-in-Deck Loading on Fixed Steel Jacket Decks. *Mar. Struct.* **2007**, *20*, 164–184. [CrossRef]
2. Karimi, H.R.; Shabakhty, N. A Comparative Assessment of the Impact of Tilting on Structural Safety and Behavior of Fixed Offshore Platforms. *Appl. Ocean Res.* **2023**, *136*, 103589. [CrossRef]

3. Abhinav, K.A.; Saha, N. Coupled Hydrodynamic and Geotechnical Analysis of Jacket Offshore Wind Turbine. *Soil Dyn. Earthq. Eng.* **2015**, *73*, 66–79. [CrossRef]

4. Damgaard, M.; Andersen, J.K.F.; Ibsen, L.B.; Andersen, L.V. Natural Frequency and Damping Estimation of an Offshore Wind Turbine Structure. In Proceedings of the International Offshore and Polar Engineering Conference, Rhodes, Greece, 17–21 June 2012; International Society of Offshore and Polar Engineers: Mountain View, CA, USA, 2012; pp. 300–307.

5. Ashford, S.A.; Juirnarongrit, T. Evaluation of Pile Diameter Effect on Initial Modulus of Subgrade Reaction. *J. Geotech. Geoenviron. Eng.* **2003**, *129*, 234–242. [CrossRef]

6. Darendeli, M.B. *Development of a New Family of Normalized Modulus Reduction and Material Damping Curves*; The University of Texas at Austin: Austin, TX, USA, 2001.

7. Jardine, R.J.; Potts, D.M.; Burland, J.B.; Fourie, A.B. Studies of the Influence of Non-Linear Stress–Strain Characteristics in Soil–Structure Interaction. *Geotechnique* **1986**, *36*, 377–396. [CrossRef]

8. Taborda, D.M.G.; Potts, D.M.; Zdravković, L. On the Assessment of Energy Dissipated through Hysteresis in Finite Element Analysis. *Comput. Geotech.* **2016**, *71*, 180–194. [CrossRef]

9. Vucetic, M.; Dobry, R. Effect of Soil Plasticity on Cyclic Response. *J. Geotech. Eng.* **1991**, *117*, 89–107. [CrossRef]

10. Ishwarya, S.; Arockiasamy, M.; Senthil, R. Inelastic Nonlinear Pushover Analysis of Fixed Jacket-Type Offshore Platform with Different Bracing Systems Considering Soil-Structure Interaction. *J. Shipp. Ocean Eng.* **2016**, *6*, 241–254. [CrossRef]

11. Zhang, X.; Far, H. *Seismic Behaviour of High-Rise Frame-Core Tube Structures Considering Dynamic Soil–Structure Interaction*; Springer: Dordrecht, The Netherlands, 2022; Volume 20, ISBN 0123456789.

12. Zhang, X.; Far, H. Effects of Dynamic Soil-Structure Interaction on Seismic Behaviour of High-Rise Buildings. *Bull. Earthq. Eng.* **2022**, *20*, 3443–3467. [CrossRef]

13. *BS EN 1998-1:2004*; Eurocode 8: Design of Structures for Earthquake Resistance. British Standards Institution: London, UK, 2004; Volume 144.

14. Benz, T. *Small-Strain Stiffness of Soils and Its Numerical Consequences*; University of Stuttgart: Stuttgart, Germany, 2007.

15. Wen, K.; Wu, X.; Zhu, B. Numerical Investigation on the Lateral Loading Behaviour of Tetrapod Piled Jacket Foundations in Medium Dense Sand. *Appl. Ocean Res.* **2020**, *100*, 102193. [CrossRef]

16. Radhima, J.; Kanellopoulos, K.; Gazetas, G. Static and Dynamic Lateral Non-Linear Pile-Soil-Pile Interaction. *Geotechnique* **2022**, *72*, 642–657. [CrossRef]

17. Prendergast, L.J.; Gavin, K. A Comparison of Initial Stiffness Formulations for Small-Strain Soil-Pile Dynamic Winkler Modelling. *Soil Dyn. Earthq. Eng.* **2016**, *81*, 27–41. [CrossRef]

18. Reese, L.C.; Welch, R.C. Lateral Loading of Deep Foundations in Stiff Clay. *J. Geotech. Eng. Div.* **1975**, *101*, 633–649. [CrossRef]

19. Souri, A.; Amirmojahedi, M.; Abu-Farsakh, M.; Voyiadjis, G.Z. Development of Unified p–y Curve Model for Clays Using Finite Element Analysis of Laterally Loaded Piles. *Can. Geotech. J.* **2023**, *60*, 1055–1072. [CrossRef]

20. Choi, J.I.; Kim, M.M.; Brandenberg, S.J. Cyclic P-y Plasticity Model Applied to Pile Foundations in Sand. *J. Geotech. Geoenviron. Eng.* **2015**, *141*, 04015013. [CrossRef]

21. Reese, L.C.; Cox, W.R.; Koop, F.D. Field Testing and Analysis of Laterally Loaded Piles Om Stiff Clay. In Proceedings of the Offshore Technology Conference, Houston, TX, USA, 5–8 May 1975.

22. Matlock, H. Correlation for Design Laterally Loaded Piles in Soft Clay. In Proceedings of the Offshore Technology Conference, Houston, TX, USA, 22–24 April 1970; pp. 577–588.

23. Zhang, Y.; Andersen, K.H. Scaling of Lateral Pile P-y Response in Clay from Laboratory Stress-Strain Curves. *Mar. Struct.* **2017**, *53*, 124–135. [CrossRef]

24. Kementzetzidis, E.; Pisanò, F.; Metrikine, A.V. A Memory-Enhanced p-y Model for Piles in Sand Accounting for Cyclic Ratcheting and Gapping Effects. *Comput. Geotech.* **2022**, *148*, 104810. [CrossRef]

25. Markou, A.A.; Kaynia, A.M. Nonlinear Soil-pile Interaction for Offshore Wind Turbines. *Wind Energy* **2018**, *21*, 558–574. [CrossRef]

26. Boulanger, R.W.; Curras, C.J.; Kutter, B.L.; Wilson, D.W.; Abghari, A. Seismic soil-pile-structure interaction experiments and analyses. *J. Geotech. Geoenviron. Eng.* **1999**, *125*, 750–759. [CrossRef]

27. Memarpour, M.M.; Kimiaei, M.; Shayanfar, M.; Khanzadi, M. Cyclic Lateral Response of Pile Foundations in Offshore Platforms. *Comput. Geotech.* **2012**, *42*, 180–192. [CrossRef]

28. Zhu, J.; Yu, J.; Huang, M.; Shi, Z.; Shen, K. Inclusion of Small-Strain Stiffness in Monotonic p-y Curves for Laterally Loaded Piles in Clay. *Comput. Geotech.* **2022**, *150*, 104902. [CrossRef]

29. Hanssen, S.B. Small Strain Overlay to the API P-y Curves for Sand. In *Rontiers in Offshore Geotechnics III: Proceedings of the 3rd International Symposium on Frontiers in Offshore Geotechnics (ISFOG 2015)*; Meyer, V., Ed.; Taylor & Francis Books Ltd.: London, UK, 2015; pp. 557–562.

30. Wen, K.; Kontoe, S.; Jardine, R.J.; Liu, T. An Axial Load Transfer Model for Piles Driven in Chalk. *J. Geotech. Geoenviron. Eng.* **2023**, *149*, 04023107. [CrossRef]

31. Wen, K.; Kontoe, S.; Jardine, R.J.; Liu, T.; Cathie, D.; Silvano, R.; Prearo, C.; Wei, S.; Schroeder, F.C.; Po, S. Assessment of Time Effects on Capacities of Large-Scale Piles Driven in Dense Sands. *Can. Geotech. J.* **2023**, *60*, 1015–1035. [CrossRef]

32. Jardine, R.J.; Buckley, R.M.; Liu, T.; Andolfsson, T.; Byrne, B.W.; Kontoe, S.; McAdam, R.A.; Schranz, F.; Vinck, K. The Axial Behaviour of Piles Driven in Chalk. *Geotechnique* **2023**, *74*, 553–569. [CrossRef]

33. Golafshani, A.A.; Bagheri, V.; Ebrahimian, H.; Holmas, T. Incremental Wave Analysis and Its Application to Performance-Based Assessment of Jacket Platforms. *J. Constr. Steel Res.* **2011**, *67*, 1649–1657. [CrossRef]

34. Wen, K. *Dynamic and Monotonic Axial Loading Responses of Piles Driven for Offshore Wind Turbines*; Imperial College London: London, UK, 2023.

35. Randolph, M.F.; Wroth, C.P. Analysis of deformation of vertically loaded piles. *J. Geotech. Eng. Div.* **1978**, *104*, 1465–1488. [CrossRef]

36. Zeng, F.; Jiang, C.; Liu, P. Cyclic P-y Curve Model of Unidirectional Loaded Pile in Sand Considering the Characteristic of Friction in the Strain Wedge Model. *Ocean Eng.* **2023**, *273*, 113998. [CrossRef]

37. Chigullapally, P.; Hogan, L.S.; Wotherspoon, L.M.; Stephens, M.; Pender, M.J. Experimental and numerical analysis of the lateral response of full-scale bridge piers. *Bull. N. Z. Soc. Earthq. Eng.* **2022**, *55*, 95–111. [CrossRef]

38. Asgarian, B.; Lesani, M. Pile-Soil-Structure Interaction in Pushover Analysis of Jacket Offshore Platforms Using Fiber Elements. *J. Constr. Steel Res.* **2009**, *65*, 209–218. [CrossRef]

39. API Recommended Practice 2A-WSD (RP 2A-WSD). *Recommended Practice for Planning, Designing and Constructing Fixed Offshore Platforms–Working Stress Design*; American Petroleum Institute: Washington, DC, USA, 2000.

40. *DNV-RP-C212*; Offshore Soil Mechanics and Geotechnical Engineering. DNV: Bærum, Norway, 2021.

41. Yee, N.C.; Johan, A.; Kajuputra, A.E.; Pangestu, L.A. Evaluation of Factors Contributing to Wave-in-Deck Using Pushover Analysis for Fixed Jacket Structures. In *IOP Conference Series: Earth and Environmental Science*; Institute of Physics Publishing: Bristol, UK, 2020; Volume 419.

42. Rahmani, A.; Taiebat, M.; Finn, W.D.L.; Ventura, C.E. Evaluation of P-y Springs for Nonlinear Static and Seismic Soil-Pile Interaction Analysis under Lateral Loading. *Soil Dyn. Earthq. Eng.* **2018**, *115*, 438–447. [CrossRef]

43. Koronides, M.; Onoufriou, T.; Michailides, C. Soil-Pile-Structure Interaction Investigation for a Marine Jetty. In Proceedings of the International Offshore and Polar Engineering Conference, Rhodes, Greece, 16–21 June 2024.

44. VTTV. *Set of Confidential Design Documents Provided by VTTV, Infrastructure Owner of the Marine Jetty of Vasiliko, Cyprus*; VTTV: Limassol, Cyprus, 2018.

45. *BS EN 1997-3 2000*; Eurocode 7. Geotechnical Design. Design Assisted by Fieldtesting. British Standards Institution: London, UK, 2000.

46. *BS EN 1997-2 2007*; Eurocode 7. Geotechnical Design. Ground Investigation and Testing. British Standards Institution: London, UK, 2007.

47. Lazarou, G.; Loukidis, D.; Bardanis, M. Seasonal Soil Moisture Changes under Mat Foundations in Nicosia Marl. In Proceedings of the 26th European Young Geotechnical Engineers Conference, Reinischkogel, Austria, 11–14 September 2018; International Society for Soil Mechanics and Geotechnical Engineering: Graz, Austria, 2018; pp. 205–214.

48. Lazarou, G.; Loukidis, D.; Bardanis, M. Moisture Migration Under Mat Foundations in Nicosia Marl. *Geotech. Geol. Eng.* **2019**, *37*, 1585–1608. [CrossRef]

49. Loukidis, D.; Bardanis, M.; Lazarou, G. Classification, Soil-Water Characteristic Curve and Swelling/Collapse Behaviour of the Nicosia Marl, Cyprus. In *E3S Web of Conferences*; EDP Sciences: Les Ulis, France, 2016; Volume 9.

50. Loukidis, D.; Lazarou, G.; Bardanis, M. Numerical Simulation of Swelling Soil—Mat Foundation Interaction. In Proceedings of the 17th European Conference on Soil Mechanics and Geotechnical Engineering (ECSMGE 2019), Reykjavik, Iceland, 1–6 September 2019; pp. 1–9.

51. *BS EN 1997-1:2004*; Eurocode 7: Geotechnical Design. British Standards Institution: London, UK, 2004.

52. Malik, M.H.; Rashid, S. Correlation of Some Engineering Geological Properties of the Murree Formation at Lower Topa (Murree District), Pakistan. *Geol. Bull. Univ. Peshawar* **1997**, *30*, 69–81.

53. Małkowski, P.; Ostrowski, Ł.; Brodny, J. Analysis of Young's Modulus for Carboniferous Sedimentary Rocks and Its Relationship with Uniaxial Compressive Strength Using Different Methods of Modulus Determination. *J. Sustain. Min.* **2018**, *17*, 145–157. [CrossRef]

54. *ABAQUS Standard User's Manual*; Dassault Systèmes Simulia Corp.: Providence, RI, USA, 2020.

55. Ramberg, W.; Osgood, W.R. *Description of Stress-Strain Curves by Three Parameters (NACA-TN-902)*; NASA: Washington, DC, USA, 1943.

56. Koronides, M. *Numerical and Field Investigation of Dynamic Soil Structure Interaction at Full-Scale*; Imperial College London: London, UK, 2023.

57. Koronides, M.; Kontoe, S.; Zdravković, L.; Vratsikidis, A.; Pitilakis, D. Numerical Simulation of SSI Free and Forced Vibration Experiments on Real Scale Structures of Different Stiffness. *Soil Dyn. Earthq. Eng.* **2023**, *175*, 108232. [CrossRef]

58. Koronides, M.; Kontoe, S.; Zdravković, L.; Vratsikidis, A.; Pitilakis, D.; Anastasiadis, A.; Potts, D.M. Numerical Simulation of Real-Scale Vibration Experiments of a Steel Frame Structure on a Shallow Foundation. In Proceedings of the 4th iInternational Conference on Performance-Based Design in Earthquake Engineering, Beijing, China, 15–17 July 2022; Wang, L., Zhang, J.-M., Wang, R., Eds.; Springer International Publishing: Cham, Switzerland, 2022; pp. 1119–1127.

59. *BS EN ISO 19901-4:2016*; Petroleum and Natural Gas Industries—Specific Requirements for Offshore Structures—Part 4: Geotechnical and Foundation Design Considerations. British Standards Institution: London, UK, 2016.

60. Vesic, A.B. Bending of beams resting on isotropic elastic solid. *J. Eng. Mech. Div.* **1961**, *87*, 35–53. [CrossRef]

61. Gazetas, G. 4th Ishihara Lecture: Soil-Foundation-Structure Systems beyond Conventional Seismic Failure Thresholds. *Soil Dyn. Earthq. Eng.* **2015**, *68*, 23–39. [CrossRef]

62. Anastasopoulos, I.; Gazetas, G.; Loli, M.; Apostolou, M.; Gerolymos, N. Soil Failure Can Be Used for Seismic Protection of Structures. *Bull. Earthq. Eng.* **2010**, *8*, 309–326. [CrossRef]

63. Drosos, V.; Georgarakos, T.; Loli, M.; Anastasopoulos, I.; Zarzouras, O.; Gazetas, G. Soil-Foundation-Structure Interaction with Mobilization of Bearing Capacity: Experimental Study on Sand. *J. Geotech. Geoenviron. Eng.* **2012**, *138*, 1369–1386. [CrossRef]

64. Mihálik, J.; Gago, F.; Vlček, J.; Drusa, M. Evaluation of Methods Based on CPTu Testing for Prediction of the Bearing Capacity of CFA Piles. *Appl. Sci.* **2023**, *13*, 2931. [CrossRef]

65. Bujnakova, P.; Kralovanec, J.; Perkowski, Z.; Bouchair, A. Verification of precast concrete girder bridge under static load. *Civ. Environ. Eng.* **2022**, *18*, 760–767. [CrossRef]

66. Vičan, J.; Gocál, J.; Odrobiňák, J. Reconstruction of the Bridge Over the Hron River in Village Hronovce. *Civ. Environ. Eng.* **2023**, *19*, 730–737. [CrossRef]

67. Kassinis, C.; Onoufriou, T.; Michailides, C. Coastal Marine Steel Corrosion: The Environment's Influence and in-Situ Monitoring-A Review. In Proceedings of the 2nd International Conference on Design and Management of Port, Coastal and Offshore Works (DMPCO 2023), Thessaloniki, Greece, 24–27 May 2023; pp. 102–106.

68. Onoufriou, T.; Michailides, C.; Christodoulides, P. Digitisation and Proactive Management of Coastal and Offshore Infrastructure and Environment. In Proceedings of the 2nd International Conference on Design and Management of Port, Coastal and Offshore Works (DMPCO 2023), Thessaloniki, Greece, 24–27 May 2023; pp. 82–86.

69. Demetriou, D.; Michailides, C.; Papanastasiou, G.; Onoufriou, T. Nowcasting Significant Wave Height by Hierarchical Machine Learning Classification. *Ocean Eng.* **2021**, *242*, 110130. [CrossRef]

70. Demetriou, D.; Michailides, C.; Papanastasiou, G.; Onoufriou, T. Coastal Zone Significant Wave Height Prediction by Supervised Machine Learning Classification Algorithms. *Ocean Eng.* **2021**, *221*, 108592. [CrossRef]